CHEMISTRY
A EUROPEAN JOURNAL

DOI: 10.1002/chem.201000320

Lanthanide(III) Complexes of 4,10-Bis(phosphonomethyl)-1,4,7,10-tetraazacyclododecane-1,7-diacetic acid (*trans*-H_6do2a2p) in Solution and in the Solid State: Structural Studies Along the Series

M. Paula C. Campello,[a] Sara Lacerda,[a] Isabel C. Santos,[a] Giovannia A. Pereira,[b, f] Carlos F. G. C. Geraldes,*[b] Jan Kotek,[c] Petr Hermann,*[c] Jakub Vaněk,[d] Přemysl Lubal,*[d] Vojtěch Kubíček,[c, e] Éva Tóth,[e] and Isabel Santos*[a]

Abstract: Complexes of 4,10-bis(phosphonomethyl)-1,4,7,10-tetraazacyclododecane-1,7-diacetic acid (*trans*-H_6do2a2p, H_6**L**) with transition metal and lanthanide(III) ions were investigated. The stability constant values of the divalent and trivalent metal-ion complexes are between the corresponding values of H_4dota and H_8dotp complexes, as a consequence of the ligand basicity. The solid-state structures of the ligand and of nine lanthanide(III) complexes were determined by X-ray diffraction. All the complexes are present as twisted-square-antiprismatic isomers and their structures can be divided into two series. The first one involves nona-coordinated complexes of the large lanthanide(III) ions (Ce, Nd, Sm) with a coordinated water molecule. In the series of Sm, Eu, Tb, Dy, Er, Yb, the complexes are octa-coordinated only by the ligand donor atoms and their coordination cages are more irregular. The formation kinetics and the acid-assisted dissociation of several Ln^{III}–H_6**L** complexes were investigated at different temperatures and compared with analogous data for complexes of other dota-like ligands. The $[Ce(\mathbf{L})(H_2O)]^{3-}$ complex is the most kinetically inert among complexes of the investigated lanthanide(III) ions (Ce, Eu, Gd, Yb). Among mixed phosphonate–acetate dota analogues, kinetic inertness of the cerium(III) complexes is increased with a higher number of phosphonate arms in the ligand, whereas the opposite is true for europium(III) complexes. According to the ^{1}H NMR spectroscopic pseudo-contact shifts for the Ce–Eu and Tb–Yb series, the solution structures of the complexes reflect the structures of the $[Ce(H\mathbf{L})(H_2O)]^{2-}$ and $[Yb(H\mathbf{L})]^{2-}$ anions, respectively, found in the solid state. However, these solution NMR spectroscopic studies showed that there is no unambiguous relation between ^{31}P/^{1}H lanthanide-induced shift (LIS) values and coordination of water in the complexes; the values rather express a relative position of the central ions between the N_4 and O_4 planes.

Keywords: crystal structures · kinetics · lanthanides · MRI contrast agents · structure elucidation

[a] Dr. M. P. C. Campello, Dr. S. Lacerda, Dr. I. C. Santos, Dr. I. Santos
Departamento de Química, Instituto Tecnológico e Nuclear
Estrada Nacional 10, 2686-953 Sacavém (Portugal)
Fax: (+351) 21-9946185
E-mail: isantos@itn.pt

[b] Dr. G. A. Pereira, Prof. Dr. C. F. G. C. Geraldes
Department of Life Sciences and Center of Neurosciences and Cell Biology
Faculty of Science and Technology, University of Coimbra
P.O. Box 3046, 3001-401 Coimbra (Portugal)
Fax: (+351) 239853607
E-mail: geraldes@bioq.uc.pt

[c] Dr. J. Kotek, Dr. P. Hermann, Dr. V. Kubíček
Department of Inorganic Chemistry
Universita Karlova v Praze (Charles University in Prague)
Hlavova 2030, 12840 Prague 2 (Czech Republic)
Fax: (+420) 22195-1253
E-mail: petrh@natur.cuni.cz

[d] J. Vaněk, P. Lubal
Department of Chemistry, Faculty of Science, Masaryk University
Kotlářská 2, 61137 Brno (Czech Republic)
Fax: (+420) 54949-2494
E-mail: lubal@sci.muni.cz

[e] Dr. V. Kubíček, É. Tóth
Centre de Biophysique Moléculaire, CNRS
Rue Charles Sadron 45071 Orléans Cedex 2 (France)
Fax: (+332) 38-63-15-17-94

[f] Dr. G. A. Pereira
Department of Chemistry, University of Aveiro
CICECO, 3810-193, Aveiro (Portugal)

Supporting information for this article is available on the WWW under http://dx.doi.org/10.1002/chem.201000320.

Introduction

Macrocycles, such as H_4dota or H_8dotp (Scheme 1) and their derivatives, form lanthanide(III) complexes that are endowed with high thermodynamic stability and kinetic inertness.[1–3] Therefore, the chemistry of lanthanide(III) complexes with these macrocyclic ligands has been extensively studied and some of them have found applications as metal carriers in biomedical research, for example, as luminescent probes,[4] NMR spectroscopic shift and/or relaxation probes,[5] as well as contrast agents for magnetic resonance imaging (MRI).[3,6–10] Some of the currently used gadolinium-based MRI contrast agents, namely, Dotarem, Gadovist and ProHance, are based on dota-like ligands. The $[Tm(dotp)]^{5-}$ complex is known as a versatile $^{23}Na^+$ NMR spectroscopic shift agent, both for perfused tissues and for in vivo animal studies.[11] More recently, radiolanthanide complexes have also been explored for imaging or therapy applications, for which purpose the labelling of clinically relevant biomolecules with dota-based bifunctional chelators has been extensively studied.[12] Although trivalent lanthanides have a similar coordination chemistry, they can form, with the same chelator, complexes that show a variety of structural characteristics, and these differences can affect their properties. A better understanding of structural parameters is of prime importance for the rational design of complexes endowed with a more favourable behaviour in various biological systems, for example, those which exhibit improved biodistribution and pharmacokinetics.[12] The structures of lanthanide(III) complexes with dota derivatives in solution as well as in the solid state have been intensively investigated.[2,3,6,9] However, solid-state structures of complexes with derivatives that have phosphorus-containing pendant arms have not been studied in so much detail, most probably due to the difficulties in getting single crystals suitable for X-ray diffraction analysis.[13–19]

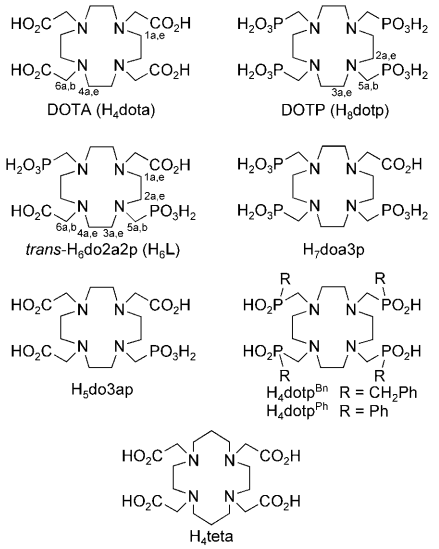

Scheme 1. Structures of the ligands. For H_6**L**, H_4dota and H_8dotp, labelling of the protons used to assign the ^{1}H NMR spectroscopic resonances is shown as well.

Generally, the structures of dota and dotp complexes are similar in a way that all ligand donor atoms are bound to the central lanthanide(III) ion in an octadentate fashion, thereby forming parallel N_4 and O_4 planes that sandwich the central ion. However, the structures of lanthanide(III) dota and dotp complexes differ in some other aspects. In solution, NMR spectroscopic studies have shown that the dota complexes are present as a mixture of two isomers that have square-antiprismatic (SA) and twisted-square-antiprismatic (TSA) structures.[20] However, the complexes of dotp and other tetraphosphorus derivatives exhibit the TSA arrangement exclusively.[13,16–18,21,22] Similarly, in the solid state, both SA and TSA structures were observed for the complexes of dota-like ligands[3,6,9] and only the TSA arrangement was found in the complexes of dotp and other tetraphosphorus derivatives.[13,16–18,21,22] Dota complexes are nona-coordinated and have one water molecule capping the O_4-plane, except for the TSA isomer of the Yb^{3+} and Lu^{3+} complexes, which have no inner-sphere water.[20a] In contrast, the coordinated water molecule is missing (except the largest lanthanide(III) ions) in the complexes of tetraphosphorus ligands.[18,22] Properties of complexes of the ligands that have one phosphorus acid and three acetic arms are similar to those of dota.[3,14,15,19,23] However, only limited data are available for Ln^{III} complexes of the dota-like ligands with other numbers (two or three) of phosphorus-containing pendant arms.[24–28]

The biological behaviour of lanthanide(III) dota and dotp complexes is also different. The dota complexes have no significant preference for any organ, but the dotp complexes and other poly(phosphonic acid) ligands exhibit a high affinity for calcified tissues.[29,30] However, the bone affinity is specific to the complexes of polyphosphonic acids, as complexes of other phosphorus-containing ligands, such as phosphinic acids[26] or phosphonic monoesters,[28,31] have no bone localisation. The complexes of monophosphorus acid dota derivatives again show biodistributions similar to those of dota complexes.[32,33]

Following our previous work on tetraazamacrocycles that bear phosphonate and/or acetate pendant arms,[13–15,25,29,30–34] we have recently reported on the synthesis and characterisation of 1,4,7,10-tetraazacyclododecane-1,7-bis(acetic acid)-4,10-bis(methylenephosphonic acid) (*trans*-H_6do2a2p, H_6**L**; Scheme 1), on its interaction with $^{153}Sm^{3+}$ and $^{166}Ho^{3+}$ ions, and on the in vitro and in vivo behaviour of these radiolanthanide complexes.[30] To get a better insight into the radiochemical and biological behaviour of these radiolanthanide complexes, we studied the complexation of *trans*-H_6do2a2p along the lanthanide series in more detail.

Herein, we report and discuss the behaviour of lanthanide(III) complexes of *trans*-H_6do2a2p in solution (thermodynamic and kinetic properties) and their structures in the solid state. A detailed analysis of lanthanide-induced shifts (LIS), based on the solid-state and NMR spectroscopic structural data, and leading to the determination of solu-

tion structures of the complexes is also presented and discussed. During the work on this project, Kálmán et al. have published some studies on the same ligand;[24] however, our study is more complete as it allows correlation of the solution and the solid-state data.

Results and Discussion

***trans*-H_6do2a2p (H_6L)—Solid-state structure and potentiometric studies**: During purification of the title ligand (see the Experimental Section), single crystals of $H_6\mathbf{L}\cdot 4H_2O$ suitable for X-ray crystallographic analysis were obtained. The molecular structure of $H_6\mathbf{L}$ is shown in Figure 1 and the

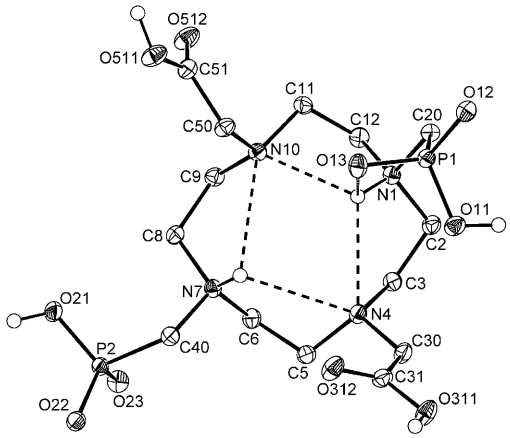

Figure 1. Molecular structure of the $H_6\mathbf{L}$ zwitterion as found in the solid-state structure of *trans*-H_6do2a2p·4H_2O.

most relevant bond lengths and angles are presented in Table S1 in the Supporting Information. The two *trans*-nitrogen atoms near the phosphonate groups (N1 and N7) are protonated, which results in NH–C_{ring} bond lengths (average 1.516 Å) longer than those around the non-protonated N4 and N10 nitrogen atoms (average N–C_{ring} bond length is 1.488 Å). Such a protonation is caused by an increase of the electronic density on the amine groups due to spreading of the negative charge of the mono-protonated phosphonate groups. Such behaviour is common for α-amino phosphonic acids,[35] and this mode of protonation has been also observed for the zwitterionic form of H_5do3ap (Scheme 1) in the solid state.[36] The two remaining protons are bound to the oxygen atoms of the two carboxylic groups, which are attached to the non-protonated nitrogen atoms. The protonation mode found in the solid state is preserved in aqueous solution as well (see below). The protonation of the carboxylate groups is confirmed by the existence of short C=O (average 1.20 Å) and long C–O (average 1.31 Å) bond lengths. The structural parameters of the phosphonate groups in $H_6\mathbf{L}$ are almost the same as those found for the zwitterionic H_5do3ap[36] and H_8dotp,[37] thereby indicating that only one oxygen atom per phosphonate group is protonated. Four nitrogen atoms of the macrocycle are almost coplanar and all pendant arms are oriented to the same side of the macrocyclic plane. One carboxylate pendant arm and one phosphonate group are positioned just above the plane due to the presence of intramolecular hydrogen bonds, whereas the other phosphonate and acetate pendant arms are oriented away from the ring to form intermolecular hydrogen bonds. The whole structure is stabilised by a network of hydrogen bonds that involve the ligand and water solvate molecules (Table S2 in the Supporting Information). This arrangement is comparable to that found for H_8dotp[37] and is different from the arrangements found for H_5do3ap[36] and $(H_5dota)^+$ cation[38] in which all four pendant arms are positioned above the N_4 plane.

To correlate ligand protonation sites found in the solid state with a protonation sequence in aqueous solution, the dependence of ^{31}P and ^{1}H chemical shifts of the N-CH_2-$PO(OH)_2$ moiety on the pH in the range $1.9 < pH < 13.8$ was followed (Figure S1 in the Supporting Information). From this dependence, values of six stepwise protonation constants ($\log K_1$ to $\log K_6$: 13.17, 12.22, 6.47, 6.44, 3.17, 2.75, respectively) were reliably determined and they are in a good agreement with those determined by potentiometry (see below). Thus, it can be concluded that the first two protonations (pH range 11–14) occur on two *trans*-nitrogen atoms N1 and N7 that bear the deprotonated phosphonate moiety. The third and the fourth ones (chemical shift changes in pH range of 5.5–7.0) occur on the phosphonate groups with a redistribution of the N–H^+ protons from N1 and N7 to N4 and N10 atoms. Finally, the next two protonations (pH range 2.0–4.0) have to occur on the carboxylate groups with another redistribution of the N–H^+ protons to the amines that bear the phosphonate groups (the protonation scheme is given in Scheme S1). The analogous redistribution of protons bound to ring nitrogen atoms as a consequence of the protonation of carboxylate/phosphorus acid pendant arms has been observed for other phosphorus-containing dota derivatives.[25,36,39]

The protonation constants of the title ligand were determined by potentiometry, except for the first constant, which had to be determined from a dependence of $^{31}P\{^1H\}$ NMR spectroscopic chemical shift on $-\log[H^+]$ under controlled conditions. The protonation constants found for $H_6\mathbf{L}$ are summarised in Table 1 and are compared with the values recently published by Kálmán et al.[24] as well as with values found in the literature for similar ligands. Figure S2 in the Supporting Information shows the corresponding species distribution diagram. The overall basicity of the nitrogen atoms ($\log K_1 + \log K_2$) of $H_6\mathbf{L}$ is higher than that of H_4dota and H_5do3ap but is lower than that of H_7doa3p and H_8dotp. Such a trend is expected, as a higher number of phosphonate groups should lead to ligands with a higher basicity.[35] However, the first dissociation constant of $H_6\mathbf{L}$ is slightly lower than the one found for H_5do3ap. The higher value found for the first dissociation constant of H_5do3ap can be explained by a different arrangement of intramolecular hydrogen bonds in the mono-protonated species of H_5do3ap

Table 1. Stepwise protonation constants ($\log K_A$)[a] of *trans*-H_6do2a2p and some related macrocyclic ligands (25 °C; for structures see Scheme 1).

Species[b]	H_6**L**[c]	H_6**L**[d]	H_4dota[e]	H_5do3ap[f]	H_7doa3p[g]	H_8dotp[h]
HL_4	13.016 *13.016(5)*[i]	12.6	11.9	13.83[i]	13.60	14.65[i]
H_2L_6	11.817 *24.833(8)*	11.43	9.72	10.35	11.42	12.40
H_3L	6.35 *31.18(1)*	5.95	4.60	6.54	7.69	9.28
H_4L	6.33 *37.513(9)*	6.15	4.13	4.34	6.33	8.09
H_5L	3.13 *40.64(1)*	2.88	2.36	3.09	5.13	6.12
H_6L	2.64 *43.28(1)*	2.77	–	1.63	2.73	5.22
H_7L	–	–	–	1.07	1.62	1.77

[a] $\text{Log}K_1 = \log\beta_1$ and $\log K_n = \log\beta_n - \log\beta_{n-1}$. [b] Charges are omitted for clarity. [c] This work (0.1 M NMe_4Cl); the experimentally determined overall protonation constants $\log\beta_n$ ($\beta_n = [H_n\mathbf{L}]/([H]^n \times [\mathbf{L}])$ are in italics. [d] Ref. [24a] (1 M KCl). [e] Ref. [40] (0.1 M NMe_4Cl). [f] Ref. [36] (0.1 M NMe_4Cl). [g] Ref. [24b] (1 M KCl). [h] Ref. [34b] (0.1 M NMe_4NO_3). [i] Determined by ^{31}P NMR spectroscopy, without control of the ionic strength.

and H_6**L**. In fact, H_5do3ap contains a rather strong intramolecular hydrogen bond that involves a protonated amine hydrogen atom and a deprotonated phosphonate group.[36] Similar behaviour has been observed for some cyclam (1,4,8,11-tetraazacyclotetradecane) derivatives with phosphorus acid pendant arms.[34b,41] The values of dissociation constants determined in this work generally agree with those determined by Kálmán et al.[24] The differences should be assigned to the difference in the background electrolyte and its concentration in these two measurements. It is known that dota-like macrocycles, and especially phosphonic acids, are able to interact with alkali metal cations,[24,36,40,42,43] which lowers the protonation constants values, and so the use of the non-complexing NMe_4^+ cation in the present work is more appropriate for the title ligand.

Thermodynamic stability of metal complexes of H_6L: We have recently reported that the radiolanthanide complexes ^{153}Sm–H_6**L** or ^{166}Ho–H_6**L** are very stable in vivo and we have found their biological behaviour to be very similar to that observed for the corresponding dota complexes (in the same animal model).[30a] To better understand the in vivo stability, we determined the stability constants of the H_6**L** complexes with Sm^{III} and Ho^{III} and with several other cations. The equilibrium constants are compiled in Table 2 and the stability constants are compared with those for other ligands in Table 3. A full set of the constants as determined from the titration experiments is given in Table S3 of the Supporting Information. Figure 2 presents the species distribution diagrams for the Ho^{III}–H_6**L** and Cu^{II}–H_6**L** systems (more distribution diagrams are shown in Figure S3).

The values of stability constants determined in this work and those of Kálmán et al.[24] are in a good agreement. The small differences are caused by the difference in ionic strength and in the values of the dissociation constants. The title ligand forms very stable complexes with trivalent lanthanides as well as with transition-metal ions. Values of stability constants of the H_6**L** complexes are intermediate in comparison with the values of the corresponding constants of the H_4dota and H_8dotp complexes. This order is caused by the differences in overall basicity of the ligands.[35] The first two protonations of the lanthanide(III) and transition-metal-ion complexes should take place on phosphonate groups and, analogously to the corresponding dota complexes, we can suppose that "in-cage" complexes are formed above pH ≈ 4. The values of dissociation constants of these protonated species are in correlation with the expected structures of the complexes. In the lanthanide(III) complexes, the phosphonate groups are coordinated and the dissociation constant values are lower than the corresponding ones in the free ligand. In the transition-metal complexes, the pendant arms can be unbound, thus leading to the higher values of the dissociation constants compared to those for lanthanide(III) complexes, in which all pendant arms are coordinated, as well as to those of the free ligand, in which the pendant arms are involved in a strong hydrogen-bond network (see above). The tetra-protonated species of the lanthanide(III) complexes should, in addition to the

Table 2. Stepwise protonation ($\log K_A$) or stability constants ($\log K_{LMn}$; $n = 1,2$) of complexes of some divalent and trivalent metal ions with H_6**L** ($I = 0.1$ M NMe_4Cl, 25 °C).

Equilibrium[a]	Equilibrium constant						
	Sm^{3+}	Ho^{3+}	Y^{3+}	Ca^{2+}	Cu^{2+}	Zn^{2+}	Cd^{2+}
$[H_2\mathbf{L}M] + 2H \rightleftharpoons [H_4\mathbf{L}M]$	"2 × 2.68"	"2 × 2.45"	"2 × 2.84"	–	–	–	2.52[b]
$[H_2\mathbf{L}M] + H \rightleftharpoons [H_3\mathbf{L}M]$	–	–	–	4.48	2.51	2.32	3.02
$[H\mathbf{L}M] + H \rightleftharpoons [H_2\mathbf{L}M]$	5.0	4.9	4.72	7.33	6.66	6.60	6.37
$[\mathbf{L}M] + H \rightleftharpoons [H\mathbf{L}M]$	6.1	5.8	5.75	8.40	7.23	7.45	7.76
$\mathbf{L} + M \rightleftharpoons [\mathbf{L}M]$	26.9	27.5	26.54	14.74	25.17	23.26	22.78
$[\mathbf{L}M_2] + H \rightleftharpoons [H\mathbf{L}M_2]$	–	3.9	3.9	6.97	5.62	–	–
$[\mathbf{L}M] + M \rightleftharpoons [\mathbf{L}M_2]$	5.5	5.5	5.48	5.15	6.19	4.47	–

[a] Charges are omitted for clarity. [b] Equilibrium constant ($\log K_A$) for equilibrium $[H_3\mathbf{L}M] + H \rightleftharpoons [H_4\mathbf{L}M]$.

Table 3. Comparison of stability constants ($\log K_{LM}$) of metal complexes with H_6**L** and with other related ligands.

Ligand	Sm^{3+}	Ho^{3+}	Y^{3+}	Ca^{2+}	Cu^{2+}	Zn^{2+}	Cd^{2+}
H_6**L**[a]	26.9	27.5	26.54	14.74	25.17	23.26	22.78
H_6**L**[b]	–	–	26.6	15.1	24.9	22.5	–
H_4dota[c]	23.0[d]	24.8[d]	24.6	17.2	22.3	20.8	21.3
H_5do3ap	28.67[e]	28.51[e]	26.0[f]	–	–	–	–
H_7doa3p[g]	–	–	–	14.50	27.3	22.9	–
H_8dotp	28.1[h]	29.2[h]	–	–	25.4[i]	–	–

[a] This work (0.1 M NMe_4Cl). [b] Ref. [24] (1 M KCl). [c] Ref. [40] (0.1 M NMe_4NO_3). [d] Ref. [44] (1.0 M NaCl). [e] Ref. [33] (0.1 M NMe_4Cl). [f] Ref. [36] (0.1 M NMe_4Cl). [g] Ref. [24b] (1.0 M KCl). [h] Ref. [45] (0.1 M NMe_4NO_3). [i] Ref. [46] (1.0 M KNO_3).

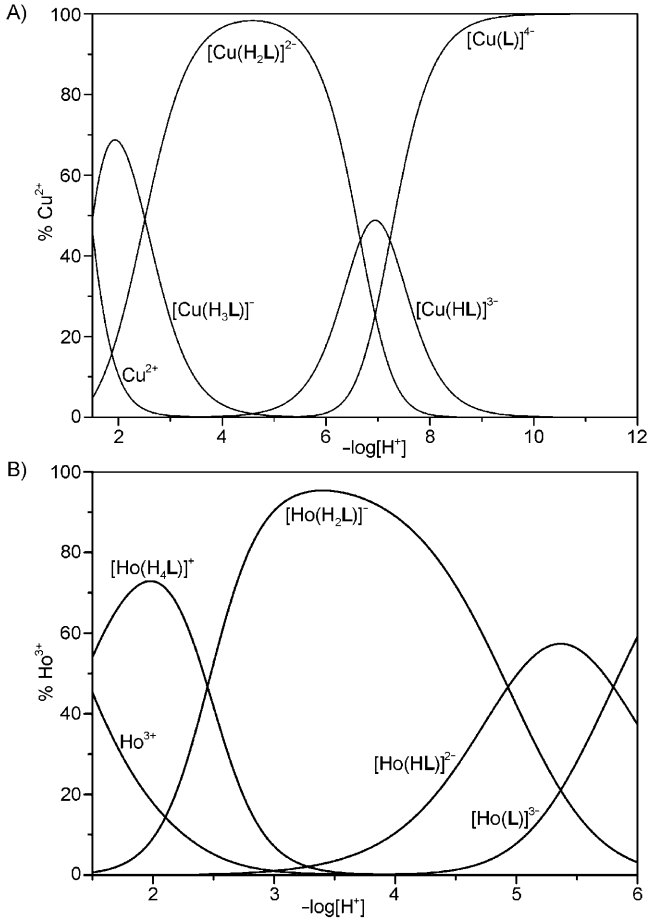

Figure 2. Species distribution diagram for the a) Cu^{II}–H_6**L** and b) Ho^{III}–H_6**L** (B) systems in **L**/M = 1:1 molar ratio ($c_L = c_M = 0.004$ M).

phosphonate groups, be protonated on two ring nitrogen atoms to form a stable "out-of-cage" complex that does not rearrange to form the "in-cage" complex in acidic solutions; such "out-of-cage" complexes of Ln^{III} with dota-like ligands have been observed in the solid state.[47,48] It also agrees with observations obtained from kinetic measurements (see below). Similar thermodynamically stable species protonated on the ring nitrogen atoms have been suggested for analogous complexes of H_5do3ap.[33,36]

The stepwise protonation constants of the preformed $[Ln(\mathbf{L})]^{3-}$ complexes (Ln = Ce, Pr, Nd, Sm, Eu, Tb, Dy, Er and Yb) were independently determined from the dependence of the ^{31}P NMR spectroscopic shift of the complexes on pH (pH range 1.2–13.5). Such determination is possible, as all the lanthanide(III) complexes are stable in a very acidic solution (pH < 2) for up to one week (evidenced by the absence of the free ligand signal in the ^{31}P NMR spectra). For all the complexes studied, only a single ^{31}P NMR spectroscopic resonance was observed over the entire pH range, thereby indicating that the protonated and deprotonated species were in a fast exchange. Such behaviour has also been observed for the $[Ln(do3ap)]^{2-}$, $[Ln(doa3p)]^{4-}$ and $[Ln(dotp)]^{5-}$ complexes.[14,25,45] Protonation of all the complexes starts at pH near 7.5, as shown by shielding of the ^{31}P NMR spectroscopic resonance of the complexes until pH near 3.7, except for the Er^{III} and Yb^{III} complexes in which deshielding occurs (Figure S4 in the Supporting Information). The δ_P of the $[Ln(\mathbf{L})]^{3-}$ complexes as a function of pH could be reliably fitted by the model including two protonation steps (i.e., it suggests the presence of the $[Ln(\mathbf{L})]^{3-}$, $[Ln(H\mathbf{L})]^{2-}$ and $[Ln(H_2\mathbf{L})]^{-}$ species in the solution). The stepwise protonation constants, $\log K_{h11}$, of the lanthanide(III) complexes determined by ^{31}P NMR spectroscopy are listed in Table 4. As can be seen in Table 4, there is no special trend along the lanthanide series for the two dissociation constants determined. Previous studies[14,25,36,45] on the $[Ln(do3ap)]^{2-}$, $[Ln(doa3p)]^{4-}$ and $[Ln(dotp)]^{5-}$ complexes have also shown that the $\log K_{h11}$ values for these complexes are insensitive to the lanthanide(III) cation, and the events have been attributed to protonations of the phosphonate group(s) coordinated to the lanthanide(III) ion. The values are in a good agreement with those determined by potentiometry, which confirms that these protonation/deprotonation steps occur on the "in-cage" complexes and they are associated with pendant phosphonate groups. Table 4 also includes the calculated ^{31}P NMR spectroscopic protonation shifts ($\Delta\delta_P$), the signs and relative absolute values of which for the different $[Ln(\mathbf{L})]^{3-}$ complexes are quite well correlated with the magnetic constants of the Ln^{III} ion (C_j^D, defined in the Supporting Information; also see Equations (7) and (8) below), indicating a progressive decrease of the pseudocontact contribution to the ^{31}P LIS values as the complex is sequentially protonated. This has been previously observed for the first two protonations of $[Ln(dotp)]^{5-}$, perhaps due to relaxation of structure of the complexes and a slight movement of the coordinated phosphonate groups away from the paramagnetic metal centre.[45]

Table 4. Stepwise protonation constants and protonation shifts $\Delta\delta_P$ for the $[Ln(\mathbf{L})]^{3-}$ complexes determined by ^{31}P NMR spectroscopy (no control of ionic strength, 21 °C).

Ln^{III} ion	$\log K_{111}$	$\log K_{211}$	$\Delta\delta_P$ (ppm)
Ce	6.1(2)	4.2(1)	−8.7
Pr	6.5(2)	4.9(2)	−41.6
Nd	6.4(1)	4.7(1)	−6.4
Sm	6.0(2)	4.8(2)	−0.4
Eu	5.2(2)	4.8(1)	−4.7
Tb	5.7(1)	5.1(2)	−356.4
Dy	5.6(1)	4.5(1)	−472.4
Er	5.6(4)	4.6(3)	50.4
Tm	_[a]	_[a]	53.8
Yb	5.3(1)	4.3(1)	41.8

[a] Not determined.

Formation of lanthanide(III) complexes: The two-step reaction mechanism has been postulated for the formation of lanthanide(III) complexes with the dota-like macrocyclic ligands. The first step is a rapid equilibrium that forms a reaction intermediate {Ln(L)}* (in which L is a general macrocyclic ligand) with the lanthanide(III) ion bound incompletely by the pendant arms (an "out-of-cage" complex). The stabil-

ity of this intermediate can be described by an equilibrium constant $K^* = [\{Ln(L)\}^*]/[Ln] \times [L]$. During the second (rate-determining) step, the "out-of-cage" species is transformed into the [Ln(L)] final product (an "in-cage" complex) and this step is determined by the individual rate constant k^* (Scheme 2A).[49,50]

$$[Ln(H_2O)_9]^{3+} + H_oL \overset{K^*}{\rightleftharpoons} \{Ln(H_2O)_x(H_pL)\}^* \xrightarrow{k^*} [Ln(H_2O)_y(H_qL)] \quad (A)$$

$$[Ln(H_2O)_9]^{3+} + H_oL \xrightarrow{{}^fk_2} [Ln(H_2O)_y(H_qL)] \quad (B)$$

Scheme 2. General scheme for the formation of the Ln^{III} complexes with dota-like ligands; the charges of ligand and complex species as well as protons and water molecules produced by the reactions are omitted for the sake of clarity.

As formation of the cerium(III) and gadolinium(III) complexes of the title ligand have already been published during the course of our work,[24] we focussed on a detailed study of the reaction mechanism of the europium(III) complex formation by means of UV spectroscopy (to follow the overall reaction, characterised by ${}^fk_2$; Scheme 2B) and steady-state/time-resolved luminescence spectroscopy (TRLS, to follow the individual step characterised by k^*). To carry out the measurements in a reasonable time with the available techniques/equipment, the experimental conditions (reactant concentrations and ratio, pH) had to be found and the measurements were carried out at several temperatures. For further study, pH 5.5 was chosen because at this value the reaction proceeds on a very convenient timescale. Below this value, the reaction is too slow because, at 24 h after mixing, the intermediate is still present; it can be seen from the value of q in Table S4 in the Supporting Information (q is the number of inner-sphere water molecules). Above this pH, the reaction is too fast to be followed by the available techniques, as the intermediate is quickly rearranged to the final product ($q < 1$, Table S4). However, the reaction mechanism is the same over the pH range 4–6 as the luminescence spectra (Figure S5) of the reaction intermediate, $\{Eu(H_2O)_x(H_p\mathbf{L})\}^*$, formed immediately after mixing of the reactants in this pH range, are the same.

The final thermodynamic Eu^{III} complex, produced by the equilibration at pH≈6, shows emission bands at 580 (electronic transition ${}^5D_0 \rightarrow {}^7F_0$), 589–595 (${}^5D_0 \rightarrow {}^7F_1$, $\Delta J = 1$) and 610 and 619 nm (${}^5D_0 \rightarrow {}^7F_2$, $\Delta J = 2$) (see Figure S5 in the Supporting Information). The $\Delta J = 2/\Delta J = 1$ band intensity ratio is approximately 1; it is between the values 1.6–1.7 reported for the H_8dotp complex and 0.65–0.75 for the H_4dota and H_5do3ap complexes.[51–53] The luminescence decay time ($\tau =$ 0.794 ms) of the Eu^{III}–$H_6\mathbf{L}$ complex in water leads to $q = 0.6 \pm 0.5$, estimated according to Choppin's formula.[54a] As this method is charged with a large uncertainty, we used Parker's formula, considered to be more accurate, for the estimation of the hydration number upon measurements in H_2O and D_2O;[54b] these measurements led to a very similar value $q = 0.5 \pm 0.2$. However, the observed value of $q \approx 0.5$ can also be interpreted as an equilibrium between non-hydrated and mono-hydrated complex molecules.[55] To exclude this possibility, we also performed a ${}^5D_0 \leftarrow {}^7F_0$ absorption study. As the spectroscopic terms with $J = 0$ are non-degenerated, it results in only one absorption band per one type of the complex environment. As the acquired spectra showed only one symmetric absorption band (Figure S6 in the Supporting Information), it means that only one type of the complex species is present in the solution. Taking into account also the luminescence measurements on europium(III) complexes of tetraphosphorus acid 1,4,7,10-tetraazacyclododecane (cyclen) derivatives in which a strong second-sphere hydration of the complexes was proven[18] and the precision of the above luminescence measurements, it can be concluded that the final product of Eu^{III} complexation has no coordinated water molecule. It also agrees with the previous ${}^{17}O$ NMR spectroscopic measurements.[24]

These preliminary measurements showed that the pH range suitable for the formation kinetics study is rather narrow (pH≈5–6). According to Scheme 2, the rate of complex formation can be expressed as Equation (1).

$$\frac{d[LnL]}{dt} = k^*[\{Ln(L)\}^*] = k^*K^*[Ln^{3+}][L] \quad (1)$$

As the luminescence lifetime of Eu^{III} complexes is proportional to the number of coordinated (inner-sphere) water molecules, q, the rate constant k^* is directly accessible by the TRLS measurements using Equation (1).[52] Alternatively, the overall reaction can be expressed as the second-order process determined by the second-order rate constant ${}^fk_2$ [Eq. (2)].

$$\frac{d[LnL]}{dt} = {}^fk_2[Ln^{3+}]_{tot}[L]_{tot} \quad (2)$$

in which $[Ln^{3+}]_{tot}$ and $[L]_{tot}$ are total concentrations of the metal- and ligand-containing species. In this case, the value of the second-order rate constant can be determined from the time dependence of absorption spectra. Reaction intermediate $\{Eu(H_2O)_x(H_p\mathbf{L})\}^*$ is formed immediately after mixing and contains around 3.5 coordinated water molecules (Figures S7 and S8 in the Supporting Information), whereas the final thermodynamic product, $[Eu(H_q\mathbf{L})]^{q-3}$, has no coordinated water molecules (see above). Combining our and the previous results,[24] the composition of the reaction intermediate is probably $\{Eu(H_2\mathbf{L})(H_2O)_{3-4}\}^{-*}$ and the protons should be bound to ring nitrogen atoms.[50,56] It can be also assumed that the structure of the reaction intermediate and the reaction mechanism are similar to those involved in reactions of the similar ligands as H_4dota,[56] H_5do3ap[52] and H_7doa3p.[25] The reaction intermediate in aqueous solution with a pH < 5.5 is not converted into the final product over the course of 24 h (Table S4 and Figure S5 in the Supporting Information). Reaction intermediate $\{Eu(H_2\mathbf{L})(H_2O)_{3-4}\}^{-*}$ is probably rearranging very slowly (days to weeks), as observed for analogous species in the Eu^{III}–H_4dota system;[56] this is probably caused by a rather high thermodynamic sta-

bility of the $\{Eu(H_2\mathbf{L})(H_2O)_{3-4}\}^{-*}$ species (Scheme 2). It is also supported by potentiometric data that suggest that the tetra-protonated species (present in solution at pH < 3), which probably has an analogous structure (two protonated ring nitrogen atoms and two mono-protonated phosphonate groups), is fully thermodynamically stable under these conditions (see above). Its equilibrium constant should be similar to that reported for the $\{Ce(H_2\mathbf{L})\}^{-*}$ complex ($\log K^* = 10.4$).[24] This value is noticeably higher than those found for the H_4dota complexes ($\log K^* = 4.5$ for $\{Ce(H_2dota)\}^{+*}$ or $\log K^* = 4.4$ for $\{Eu(H_2dota)\}^{+*}$)[49] as well as for the H_5do3ap complexes ($\log K^* = 3.45$ for $\{Ce(H_3do3ap)\}^{+*}$ or $\log K^* = 3.0$ for $\{Eu(H_3do3ap)\}^{+*}$).[36,52]

In a comparison of the rate of rearrangement of the $\{Ln(H_pdota)\}^*$ and $\{Ln(H_p\mathbf{L})\}^*$ reaction intermediates, the former one is more stable at a lower pH. The rate constant of conversion of the $\{Eu(H_2\mathbf{L})(H_2O)_{3-4}\}^{-*}$ intermediate complex, $k^* = 2.09(6) \times 10^{-4}\ s^{-1}$ (25 °C, $c_{Eu} = c_L \approx 0.005$ M, Table 5), is also one order of magnitude lower than that for the intermediate Eu^{III} complex with H_5do3ap ($4.7 \times 10^{-3}\ s^{-1}$)[52] measured under identical conditions. Surprisingly, a faster reaction with the rate constant $k^* = 5.9(4) \times 10^{-4}\ s^{-1}$ (25 °C, Table 5, Figure S7 in the Supporting Information) was observed in reactant concentrations that were ten times lower ($c_{Eu} = c_L \approx 0.0005$ M). This observation can be explained by a formation of polymeric complexes in which phosphonate groups bridge the metal ions to form multinuclear species, as has been observed for the Ln^{III}–H_8dotp complexes in solution[21a] and in the solid state[57] as well as for lanthanide(III) complexes of other tetraphosphorus dota analogues.[22] The polymer formation effectively competes with conversion of the (polymeric) intermediate into the final "in-cage" complex and it is more pronounced under higher overall concentrations of reactants.

Table 5. The results of UV/Vis ($^fk_2$) and TRLS (k^*) measurements on the Eu^{III}–$H_6\mathbf{L}$ system (pH 5.5, $c_{Eu} = c_L \approx 0.0005$ M).

Temperature [°C]	$^fk_2$ [$M^{-1}s^{-1}$] [a]	q_{EuL^*} [b,c]	q_{EuL} [b,c]	k^* [$10^{-4}s^{-1}$] [b]
20.0	0.477(3)	3.56(4)	0.57(2)	5.0(2)
25.0	0.831(8)	3.46(8)	0.73(4)	5.9(4)
		3.28(3)[d]	0.98(2)[d]	2.09(6)[d]
30.0	1.558(7)	3.57(7)	0.53(3)	14.8(9)
35.0	3.647(20)	3.90(13)	0.63(5)	24.4(2)
40.0	8.129(70)	2.27(8)[e]	0.56(4)	75.4(15)
Activation parameters				
E_a [kJ mol^{-1}]	109(7)			104(14)
$\Delta H^{\neq}$ [kJ mol^{-1}]	106(7)			102(14)
$\Delta S^{\neq}$ [J K^{-1} mol^{-1}]	111(22)			37(48)

[a] UV measurements. [b] TRLS measurements. [c] The errors in parentheses correspond to a fitting of the time vs. q dependence; q in any time point was determined by Choppin's method[54] with precision of ±0.5 H_2O. [d] $c_{Eu} = c_L = 0.005$ M. [e] Rough estimate due to a fast formation reaction.

Generally, the overall formation rate characterised by $^fk_2 = 0.83\ M^{-1}s^{-1}$ (measured under analogous conditions) is slower than that for the $[Gd(dota)]^-$ complex ($^fk_2 = 205\ M^{-1}s^{-1}$)[58] but somewhat faster than for the $[Eu(doa3p)]^{4-}$ complex ($^fk_2 = 0.21\ M^{-1}s^{-1}$).[25]

With increasing temperature, the metal-transfer reaction step is accelerated. This transformation process, followed by TRLS and absorption spectroscopy in the UV region, was studied at different temperatures (Figure S7 in the Supporting Information and Table 5) and its rate constant and thermodynamic and activation parameters were calculated. The results are compiled in Table 5. The activation energy parameters for the transformation process characterised by the rate constant k^* are comparable with the values calculated for a formation of the Ce^{III} complexes with analogous ligands at pH 5.5 ($E_a = 83$ kJ mol^{-1}, $\Delta H^{\neq} = 80$ kJ mol^{-1} for the Ce^{III}–H_4dota and $E_a = 108$ kJ mol^{-1}, $\Delta H^{\neq} = 105$ kJ mol^{-1} for the Ce^{III}–H_4teta (Scheme 1) systems, respectively).[59] In addition, the thermodynamic parameters for formation of the reaction intermediate, $\{Eu(H_2\mathbf{L})(H_2O)_{3-4}\}^{-*}$, were calculated (for K^*: $\Delta H^0 = 5$ kJ mol^{-1}, $\Delta S^0 = 74$ J K^{-1} mol^{-1}). Thus, formation of the reaction intermediate shows an athermic character. It can be explained by the fact that coordinated water molecules in the Eu^{III}–aqua complex are replaced with the pendant arms that have the same donor (oxygen) atoms; this process does not bring any enthalpic gain. The large entropy change implies a high number of particles evolved over the course of the reaction (the dissociation of water molecules from Eu^{III}–aqua complex due to the ligand coordination). Analogous data for K^* have been observed in the Ce^{III}–H_4teta system.[59]

Dissociation of lanthanide(III) complexes: The dissociation of lanthanide(III) complexes can be written as Equation (3):

$$-\frac{d[Ln(L)]}{dt} = {}^dk_{obs}[Ln(L)]_{tot} \quad (3)$$

In the commonly accepted dissociation mechanism, the initial fast protonation(s) of the complex species (on the pendant arm(s)) is followed by a rate-determining rearrangement step that is connected with a proton transfer to a macrocycle amino group, with the simultaneous cleavage of the Ln–N bonds to form an intermediate complex $[\{Ln(H_n\mathbf{L})\}^*]^{x+}$ (see Scheme 3). Such a process is followed by a fast cleavage of other coordination bonds and simultaneous

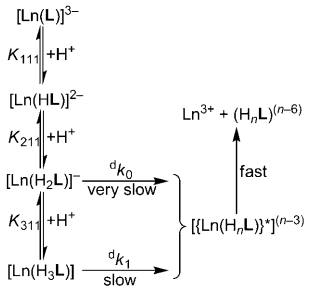

Scheme 3. Proposed mechanism of the acid-assisted dissociation of the $[Ln(\mathbf{L})]^{3-}$ complexes.

protonation of other amino groups, which leads to the complex dissociation.

According to the observed dissociation constants of the Ln^{III}–$H_6\mathbf{L}$ complex species and the corresponding distribution diagrams (see Figure 2 and Tables 2–4 above, and Table S3 in the Supporting Information), one can assume that the major species present at pH ≈ 3 is the double-protonated complex. The first two stepwise protonation constants of these lanthanide(III) complexes are 5.3–6.5 ($\log K_{111}$) and 4.2–5.1 ($\log K_{211}$); these processes lead to mono-protonation on each phosphonate pendant arm and the protonated species are fully thermodynamically stable. Therefore, the pre-dissociation protonation step is probably connected with the formation of the $[Ln(H_3\mathbf{L})]$ complex in which the third proton is located on the uncoordinated oxygen atom of carboxylate or phosphonate pendant arm. This species undergoes the dissociation reaction described in Scheme 3. The corresponding rate law is given by Equation (4) and has usually been used for a description of the acid-assisted dissociation of lanthanide(III) complexes of macrocyclic dota-like ligands.[1,24]

$$ {}^{d}k_{obs} = \frac{{}^{d}k_0 + {}^{d}k_1 K_{311}[H^+]}{1 + K_{311}[H^+]} \quad (4) $$

In some cases, when $K \times [H^+] \ll 1$ (i.e., if the protonation constant is very low and/or at a low proton concentration; here $K = K_{311}$) and the spontaneous dissociation (characterised by ${}^{d}k_0$) is too slow, the generalised Equation (4) can be rewritten in a simpler form as Equation (5).

$$ {}^{d}k_{obs} = {}^{d}k_1 K_{311}[H^+] = k_H[H^+] \quad (5) $$

The acid-assisted dissociation of several lanthanide(III) complexes was studied in the region of $[H^+] = 0.05$–3.00 M adjusted by perchloric acid. The UV/Vis spectrum of the $[Ce(H_2O)(\mathbf{L})]^{3-}$ complex shows a maximum at 310 nm that disappears during the course of the dissociation reaction (Figure S9 in the Supporting Information) and it fits into the series of $[Ce(H_2O)(dota)]^-$ (319 nm),[49] $[Ce(H_2O)(do3ap)]^{2-}$ (313 nm),[36] $[Ce(H_2O)(doa3p)]^{4-}$ (305 nm)[24,25] and $[Ce(H_2O)(dotp)]^{5-}$ (300 nm)[60] complexes. Figure 3 shows the example of dependence of the observed pseudo-first-order rate constant, ${}^{d}k_{obs}$, of the Ce^{III}–$H_6\mathbf{L}$ complex on the acidity of solution and temperature. The other example, dissociation of the Eu^{III}–$H_6\mathbf{L}$ complex at different proton concentrations, can be found in Figure S10. The parameters according to Equation (4) were calculated and the results are given Table 6.

To get more information about differences in kinetic inertness of the lanthanide(III) complexes, the acid-assisted dissociation was studied for Ce^{III}, Eu^{III}, Gd^{III} and Tb^{III} complexes under identical conditions ($I = 3.0$ M, 50 °C). The dependences of ${}^{d}k_{obs}$ on the solution acidity are shown in Figure 4 and the parameters calculated according to Equation (4) are given in Table 6. The dependence of ${}^{d}k_{obs}$ on

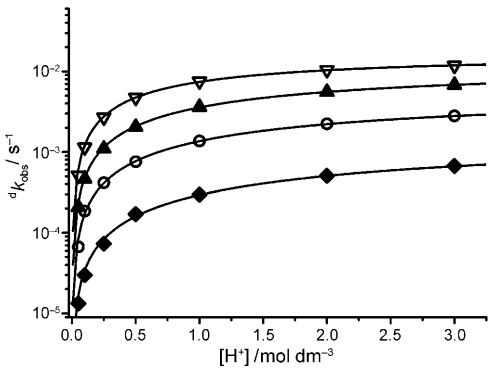

Figure 3. Dependence of the observed pseudo-first-order rate constant of the acid-assisted dissociation (${}^{d}k_{obs}$) of the $[Ce(H_2O)(\mathbf{L})]^{3-}$ complex on solution acidity at different temperatures ($I = 3.0$ M (H,Na)ClO_4; ◆ = 25, ○ = 40, ▲ = 50 and ▽ = 60 °C).

Table 6. Kinetic parameters for acid-assisted decomplexation of the $[Ln(\mathbf{L})]^{3-}$ complexes according to Equation (4) ($I = 3.0$ M (H,Na)ClO_4; in all cases, ${}^{d}k_0$ was found to be zero).

Temperature [°C]	$k_H (= {}^{d}k_1 \times K_{311})$ [10^{-4} M^{-1} s^{-1}]	K_{311} [M^{-1}]	${}^{d}k_1$ [10^{-3} s^{-1}]
Ce^{III}			
25.0	3.5 ± 0.1	0.193 ± 0.018	1.81 ± 0.18
40.0	17.7 ± 0.7	0.300 ± 0.010	5.90 ± 0.30
50.0	50.0 ± 0.7	0.400 ± 0.013	12.50 ± 0.44
60.0	131.3 ± 3.0	0.771 ± 0.029	17.03 ± 0.75
Activation or thermodynamic parameters			
E_a [kJ mol^{-1}]	85.6 ± 0.6	–	54.5 ± 5.3
ΔH [kJ mol^{-1}]	$\Delta H^{\neq} = 83.0 \pm 0.6$	$\Delta H^0 = 31.1 \pm 5.7$	$\Delta H^{\neq} = 51.9 \pm 5.3$
ΔS [J K^{-1} mol^{-1}]	$\Delta S^{\neq} = -32.9 \pm 1.8$	$\Delta S^0 = 89.8 \pm 17.9$	$\Delta S^{\neq} = -122.7 \pm 16.9$
Eu^{III}			
25.0	5.2 ± 0.3	1.64 ± 0.13	0.317 ± 0.031
40.0	33.2 ± 5.9	2.34 ± 0.55	1.42 ± 0.42
50.0	85.4 ± 10.1	2.31 ± 0.36	3.70 ± 0.72
60.0	165.0 ± 20.0	1.83 ± 0.30	9.0 ± 1.8
Activation or thermodynamic parameters			
E_a [kJ mol^{-1}]	82.5 ± 5.9	–	79.0 ± 0.5
ΔH [kJ mol^{-1}]	$\Delta H^{\neq} = 79.9 \pm 6.0$	$\Delta H^0 = 4 \pm 17$	$\Delta H^{\neq} = 76.4 \pm 0.5$
ΔS [J K^{-1} mol^{-1}]	$\Delta S^{\neq} = -38.8 \pm 19$	$\Delta S^0 = 6 \pm 20$	$\Delta S^{\neq} = -55.7 \pm 1.5$
Gd^{III}			
50.0	207.5 ± 32.1	5.8 ± 1.1	3.57 ± 0.87
Tb^{III}			
50.0	270.8 ± 23.5	4.72 ± 0.49	5.73 ± 0.7

proton concentration observed in the case of Ce^{III} has a different shape from those for other lanthanide(III) ions (Figure 4); however, it just corresponds to a much lower value of the protonation constant K_{311} compared to the complexes of the other ions (about one order of magnitude; see Table 6). Such an observation might be explained by structural differences between the complexes of cerium(III) and the other lanthanide(III) ions (see below for the solid-state structures). As the Ce^{III} ion has the largest ionic radius, it is able to form nona-coordinated complexes (with an apical inner-sphere water molecule) even with tetrakis(methyl-

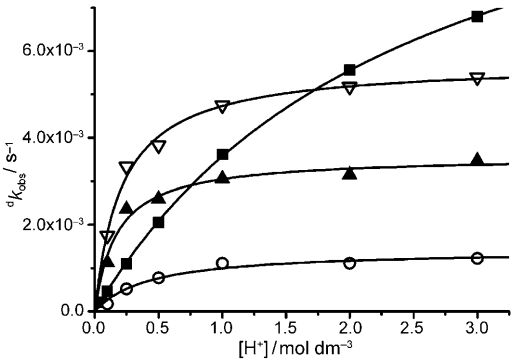

Figure 4. Dependence of observed pseudo-first-order rate constant of the acid-assisted dissociation ($^{d}k_{obs}$) of the $[Ln(\mathbf{L})]^{3-}$ complexes on solution acidity (50 °C, $I=3.0$ M (H,Na)ClO_4; ■ = Ce, ○ = Eu, ▲ = Gd and ▽ = Tb).

phosphorus acid) cyclen derivatives.[17] The cerium(III) complex is harder to protonate to get kinetically important triprotonated species; it leads to a lower $\log K_{311}$ value. But once the complex is protonated it decomposes faster than the other ones ($^{d}k_1$ in Table 6), possibly due to a better exposure of the central ion to solvent. Such considerations are also supported by the fact that this protonation process for the $[Ce(H_2\mathbf{L})(H_2O)]^-$ complex is largely endothermic because the access to the next proton is blocked, probably due to presence of a system of hydrogen bonds that involve the inner-sphere water molecule. The same process for the $[Eu(H_2\mathbf{L})(H_2O)]^-$ complex is athermic.

Table 7. Kinetic parameters for acid-assisted decomplexation of the $[Ln(\mathbf{L})]$ complexes [according to Equation (4); 25 °C, $I=3.0$ M (Na,H)ClO_4].

Ligand	k_H [10^{-4} M^{-1}s^{-1}]	K [M^{-1}]	$^{d}k_1$ [10^{-4}s^{-1}]	$^{d}k_{obs}$ [10^{-6}s^{-1}] ([H$^+$]=0.01 M)	$^{d}k_{obs}$ [10^{-4}s^{-1}] ([H$^+$]=3.0 M)	Ref.
Ce^{III}						
H_4dota	8; 20[a]	–	–	8.2[a]	204[a]	[49]
H_5do3ap	12.2	–	–	12	36.6	[36]
trans-H_6do2a2p	3.5	0.19	18	3.5	6.71	this work
H_7doa3p	2.4	0.92	3.0	2.4	1.91	[25]
H_8dotp	0.46	3.3[b]	–	0.46	1.18	[60]
Eu^{III}						
H_4dota[c]	0.14; 10	14; 0.12	0.01; 6.2	0.21	1.6	[49]
H_5do3ap	0.98	0.21	4.6	0.96	1.8	[52]
trans-H_6do2a2p	5.2	1.64	3.2	5.1	2.6	this work
H_7doa3p	2.35	0.29	8.0	2.3	4.1	[25]
H_8dotp	9.8	2.0	6.2	12.7	5.6	[53]

[a] $k_{obs}=k_{H1}\times[H^+]+k_{H2}\times[H^+]^2$. [b] 50 °C. [c] $k_{obs}=\frac{k_{d1}\times K_1\times[H^+]+k_{d2}\times K_1\times K_2\times[H^+]^2}{1+{}^{H}K_1\times[H^+]+{}^{H}K_1\times{}^{H}K_2\times[H^+]^2}$.

The completeness of the acid-assisted complex dissociation of the Eu^{III} complex was studied by luminescence spectroscopy. The average number of water molecules coordinated to the Eu^{III} ion slowly increases with time (Figure S11 in the Supporting Information) as the fluorescence intensity of both $^5D_0\rightarrow{}^7F_1$ and $^5D_0\rightarrow{}^7F_2$ emission bands simultaneously decreases. It is caused by a slow release of the Eu^{III} ion from the macrocyclic cavity. Measurements of the luminescence emission spectra and the luminescence decay time confirmed that the dissociation reaction is finished in about 4–5 h and the final product is the $[Eu(H_2O)_9]^{3+}$ ion (25 °C, 3 M $HClO_4$).

A key role in the evaluation of the acid-assisted dissociation is given by the value of k_H; at 50 °C, it increases along the lanthanide series with similar activation parameter values (Table 6). However, at laboratory temperature, this behaviour changes and the value of k_H for the $[Ln(\mathbf{L})]^{3-}$ complexes with lighter lanthanides is slightly higher than that for the $[Gd(\mathbf{L})]^{3-}$ complex ($k_H=3.5\times10^{-4}$ M^{-1}s^{-1} for Ce^{III} and 5.2×10^{-4} M^{-1}s^{-1} for Eu^{III} vs. 1.95×10^{-4} M^{-1}s^{-1} for Gd^{III},[24] respectively).

The reactivity of the Ce^{III} and Eu^{III} complexes of H_4dota, H_5do3ap, $H_6\mathbf{L}$, H_7doa3p and H_8dotp can be compared (as measurements were done under the same experimental conditions) through the rate constant k_H (Table 7). The values change with an increasing number of phosphonic acid pendant arms; they decrease for the Ce^{III} and increase for the Eu^{III} complexes. For the Gd^{III} complexes, an analogous order was not found.[24] The order of kinetic inertness of the lanthanide(III) complexes can be possibly explained from a structural point of view. All Ce^{III} complexes probably contain one coordinated water molecule, which may participate in a hydrogen-bond network with the protonated phosphonate groups. Then, access of the next proton to already mono-protonated phosphonate group(s) is better blocked when more phosphonate groups are present. On the other hand, the order of inertness of the Eu^{III} complexes is the opposite of the Ce^{III} ones. Because the complexes of $H_6\mathbf{L}$ and H_8dotp with the smaller Eu^{III}, Gd^{III} and Tb^{III} ions do not contain coordinated water molecule, the proton transfer into the coordination cage is easier and therefore the complexes of ligands with more phosphonate groups are less inert.

Structural analysis of lanthanide(III) complexes in the solid state: Single crystals of the Ln^{III}–$H_6\mathbf{L}$ complexes (Ln = Ce, Nd, Sm, Eu, Tb, Dy, Er and Yb) suitable for X-ray analysis were obtained by slow vapour diffusion of a *i*PrOH/EtOH (1:1) mixture into an aqueous solution of the complexes at pH ≈ 4.5 (in which mostly the diprotonated species should be present, Figure 2) over the course of 3–4 months at room temperature. In all the complexes, the usual features of lanthanide(III) complexes of dota-like ligands are preserved.[3] The tetraazamacrocyclic ring displays a quadrangular [3333] conformation and four nitrogen (thus forming an N_4 plane) and four oxygen (one from each pendant arm;

that is, two from acetate and two from phosphonate groups, thus forming an O_4 plane) atoms of the ligand are bound to the central ions. The O_4 and N_4 planes are parallel (Table 8). The same sign of the rotation of the pendant arms and of the conformation of macrocyclic chelate rings lead to an exclusive formation of the Λλλλλ/Δδδδδ enantiomeric pair, which is usually labelled as a "twisted-square-antiprismatic" (TSA) diastereoisomer. Mean twist angles ω of the pendant arms (for a definition of the structural parameters, see Figure S12 in the Supporting Information) change in the range of 22.8–28.3° and therefore is also consistent with TSA isomers (theoretical value of 22.5° compared to 45° for a square-antiprismatic arrangement). Generally, bond lengths between the central ions and the donor atoms of the title ligand are in the range expected for this type of complexes.

In the isostructural compounds $K[Ln(H_2\mathbf{L})(H_2O)]\cdot KCl\cdot 5H_2O$ (Ln = Ce and Nd), the central ion is nona-coordinated; eight donor atoms come from the ligand and one from a water molecule that caps the O_4 plane (Figure 5). The opening angles ϕ (Figure S12 in the Supporting Information) are higher than the limiting value of 135°, thereby assuring enough space for water molecule coordination.[3,14,15,19,35] Systematically, the angles ϕ between phosphonate pendant arms are about 7° (Table 8) lower than those between carboxylates. In these two complexes, each phosphonate group is mono-protonated (corresponding protons were located in the difference electron map). This feature is also evident from differences in P–O bond lengths; P1–O2 and P2–O7 are longer (≈1.57 Å) than the other P–O bonds (≈1.50 Å). The complex molecules form zigzag chains by means of the coordination of carboxylate and phosphonate oxygen atoms to potassium(I) ions. The coordination chains form warped planes in the *xz* direction, with solvate water molecules and chloride anions placed between these planes (Figure S13). Similarly, one of the Sm^{III} complexes, $K_3[Sm(H_2\mathbf{L})(H_2O)][Sm(H\mathbf{L})(H_2O)]\cdot KCl\cdot 16H_2O$, contains the apically bound water molecule as well. In this structure, two independent complex units were found that show the same binding mode and a very close geometry (Table 8, Figure S14 in the Supporting Information). The first of the complex molecules is double-protonated, whereas the second one only mono-protonated. Such a protonation scheme is also reflected by P–O bond lengths. In the crystal structure, the complex units are connected through potassium(I) ions into a two-dimensional coordination polymer, thereby forming planes in the *xz* direction (Figure S15 in the Supporting Information). Lengths between the Ln^{III} ion and the coordinated water molecule, $Ln–O_w$, are similar for the Ce^{III} and Nd^{III} complexes and for one molecule of the Sm^{III} complex (≈2.55 Å); for the other independent molecule found in the same Sm^{III} structure, the length is slightly longer (≈2.60 Å). These values lie in the range of those found for the series of $[Ln(dota)(H_2O)]^-$ (2.42–2.59 Å) and $[Ln(Hdo3ap)(H_2O)]^-$ (2.50–2.68 Å) complexes.[14,15,61]

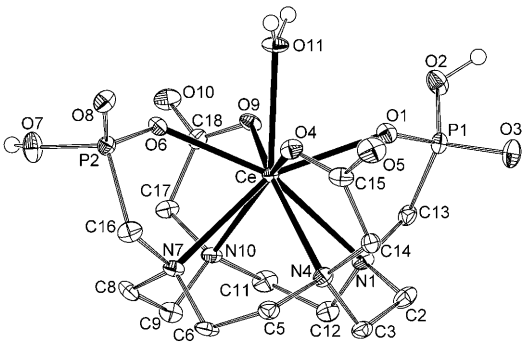

Figure 5. Molecular structure of the $[Ce(H_2\mathbf{L})(H_2O)]^-$ anion found in the structure of $K[Ce(H_2\mathbf{L})(H_2O)]\cdot KCl\cdot 5H_2O$. Hydrogen atoms bound to carbon atoms are omitted.

In the second isostructural series, $K_2[Ln(H\mathbf{L})]\cdot 6.5H_2O$, with smaller lanthanides (Ln = Sm, Eu, Tb, Dy, Er and Yb), the central ion is only octa-coordinated by the ligand donor atoms. There is not enough space for apical water coordination, as the values of the opening angle (ϕ) (P)O-Ln-O(P) are much lower than the border value of approximately 135° that is crucial for water binding (Table 8).[3,14,15,19,35] However, there is a large difference in the values of ϕ between phosphonate and carboxylate groups. The opening angles (ϕ) are 131–136° for the carboxylate pendant arms but the values are about 20° smaller for the (P)O-Ln-O(P) angles (113–116°). This structural feature pushes central ions deeper into the ligand cavity (see $Ln–QN_4$ lengths) and, together with the absence of coordinated water molecule, it leads to longer $Ln–QO_4$ lengths (Table 8). The molecules of the complexes possess a crystallographic two-fold symmetry and are connected into chains through a very short symmetric hydrogen bond ($d(O\cdots O') = 2.40$ Å). This hydrogen bond is reflected also in differences in the P–O bond lengths between protonated oxygen atom (P1–O2 ≈ 1.53 Å) and the second one with the phosphoryl group character (P1–O3 ≈ 1.50 Å). As an example, Figure 6 shows the molecular structure of the Dy^{III} complex. The complex chains are connected into double chains by coordination bonds to counter potassium(I) cations (Figure S16 in the Supporting Information). In the crystal structure of $K_2[Eu(H\mathbf{L})]\cdot 6.5H_2O$, a huge disorder in the complex molecule was found (Figure S17 in the Supporting Information), which leads to relatively poor statistical parameters of the refinement. However, it is obvious that this compound is isostructural with others in the series. Due to the disorder, the calculated lengths and bond angles are loaded with a high error, but their values are very reasonable and fall into the trends of the values found in the other structures (Table 8).

In general, the central ions lie closer to the O_4 plane (≈0.8 Å) in the nona-coordinated hydrated species (TSA) than in the octa-coordinated ones (TSA′, ≈1.1 Å) (Table 8).[3,15,35] Although the conformation of the macrocycle is the same over the whole series and the ligand cage represented as $d(QN_4–QO_4)$ also remains the same along the series (Table 8), the twist angles change significantly. In the case of TSA species, the twist angle of methylphospho-

Table 8. Selected bond lengths [Å], bond angles [°] and other molecular parameters for the lanthanide(III) complexes of *trans*-H_6do2a2p.

Compound	K[Ce(H_2**L**)(H_2O)]·KCl·5H_2O	K[Nd(H_2**L**)(H_2O)]·KCl·5H_2O	K_3[Sm(H_2**L**)(H_2O)][Sm(H**L**)(H_2O)]·KCl·16H_2O[a]	K_2[Sm(H**L**)]·6.5H_2O	K_2[Eu(H**L**)]·6.5H_2O[b]
d(Ln–N1)	2.797(4)	2.762(6)	2.726(7)/2.718(7)	2.630(2)	2.693(21)/2.660(30)
d(Ln–N4)	2.720(4)	2.709(6)	2.692(6)/2.695(7)	2.631(2)	2.630(18)/2.600(29)
d(Ln–N7)	2.784(4)	2.769(6)	2.705(6)/2.752(7)	–	–
d(Ln–N10)	2.753(4)	2.727(6)	2.687(7)/2.709(7)	–	–
mean *d*(Ln–N)	2.765	2.742	2.703/2.719	2.631	2.662/2.630
d(Ln–QN_4)[c]	1.774	1.749	1.715/1.729	1.584	1.616/1.615
d(Ln–O1)	2.406(4)	2.384(5)	2.341(5)/2.342(5)	2.298(2)	2.318(15)/2.296(22)
d(Ln–O4)	2.501(3)	2.476(5)	2.393(5)/2.375(5)	2.396(2)	2.414(13)/2.434(20)
d(Ln–O6)	2.411(4)	2.384(5)	2.346(5)/2.343(5)	–	–
d(Ln–O9)	2.480(3)	2.450(5)	2.422(5)/2.423(5)	–	–
mean *d*(Ln–O)	2.450	2.424	2.376/2.371	2.347	2.366/2.365
d(Ln–O_w)	2.545(4)	2.542(5)	2.555(6)/2.602(5)	–	–
d(Ln–QO_4)[c]	0.822	0.835	0.801/0.819	1.063	1.101/1.086
d(QN_4–QO_4)[c]	2.596	2.584	2.516/2.547	2.647	2.716/2.700
twist angles ω					
pendant(N1)	−26.4(1)	−26.9(2)	−30.0(3)/−27.7(3)	−20.8(1)	−19.6(8)/19.7(1.0)
pendant(N4)	−21.9(2)	−23.1(2)	−27.1(3)/−25.9(3)	−24.7(1)	−25.1(7)/23.2(1.1)
pendant(N7)	−26.1(1)	−26.5(2)	−29.1(3)/−28.2(3)	–	–
pendant(N10)	−21.9(2)	−22.8(2)	−27.0(3)/−25.8(3)	–	–
mean ω	−24.1	−24.8	−28.3/−26.9	−22.8	−22.4/21.5
opening angles ϕ (O-Ln-O)					
ϕ(phosphonates)	136.9(1)	136.1(2)	137.4(2)/135.3(2)	116.3(1)	115.5(7)/115.1(1.0)
ϕ(carboxylates)	144.4(1)	143.2(2)	143.8(2)/143.8(2)	135.2(1)	132.9(7)/134.6(1.0)
N_4–O_4 angles					
planeN_4–planeO_4	0.92(1)	0.89(1)	0.26(8)/0.96(9)	0.00	0.00/0.00
QN_4-Ln-QO_4[c]	178.4	178.2	179.0/177.7	180.0	180.0/180.0

Compound	K_2[Tb(H**L**)]·6.5H_2O	K_2[Dy(H**L**)]·6.5H_2O	K_2[Er(H**L**)]·6.5H_2O	K_2[Yb(H**L**)]·6.5H_2O
d(Ln–N1)	2.615(5)	2.581(3)	2.580(4)	2.565(3)
d(Ln–N4)	2.592(6)	2.575(3)	2.568(4)	2.560(3)
d(Ln–N7)	–	–	–	–
d(Ln–N10)	–	–	–	–
mean *d*(Ln–N)	2.604	2.578	2.574	2.563
d(Ln–QN_4)[c]	1.552	1.532	1.524	1.507
d(Ln–O1)	2.271(4)	2.246(2)	2.244(3)	2.218(2)
d(Ln–O4)	2.369(5)	2.334(2)	2.330(3)	2.314(3)
d(Ln–O6)	–	–	–	–
d(Ln–O9)	–	–	–	–
mean *d*(Ln–O)	2.320	2.290	2.287	2.266
d(Ln–O_w)	–	–	–	–
d(Ln–-QO_4)[c]	1.079	1.077	1.086	1.094
d(QN_4–QO_4)[c]	2.631	2.610	2.610	2.601
twist angles ω				
pendant(N1)	−21.5(2)	−22.2(1)	−23.4(2)	−23.4(1)
pendant(N4)	−25.2(2)	−25.3(1)	−26.0(2)	−25.7(1)
pendant(N7)	–	–	–	–
pendant(N10)	–	–	–	–
mean ω	−23.4	−23.8	−24.7	−24.6
opening angles ϕ (O-Ln-O)				
ϕ(phosphonates)	114.7(2)	114.4(1)	114.5(2)	113.0(1)
ϕ(carboxylates)	133.6(2)	132.6(1)	131.4(2)	130.8(1)
N_4–O_4 angles				
planeN_4–planeO_4	0.00	0.00	0.00	0.00
QN_4-Ln-QO_4[c]	180.0	180.0	180.0	180.0

[a] Two independent molecules in the elementary unit ([Sm(H_2**L**)(H_2O)]$^-$/[Sm(H**L**)(H_2O)]$^{2-}$ fragments). [b] Two disordered parts of the complex molecule (more abundant part Λλλλλ/less abundant part Δδδδδ). [c] QN_4 and QO_4 are centroids of the N_4 and O_4 planes, respectively.

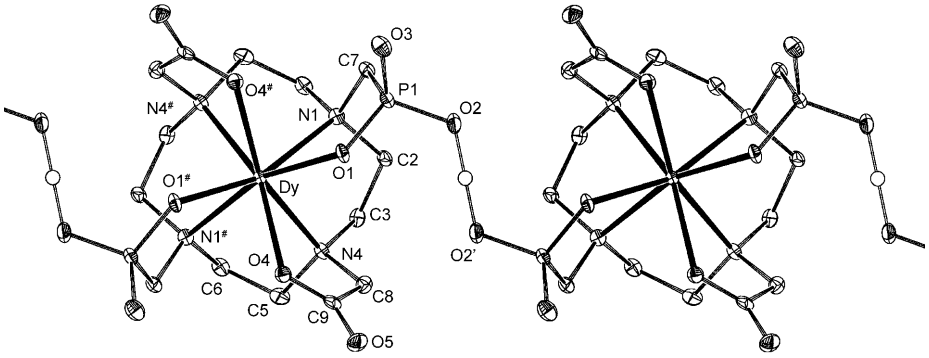

Figure 6. The motif of hydrogen-bond connections between $[Dy(H\mathbf{L})]^{2-}$ complex units found in the structure of $K_2[Dy(H\mathbf{L})]\cdot 6.5\,H_2O$. Hydrogen atoms bound to carbon atoms are omitted.

nate arm is much larger (≈27–30°) than in the octa-coordinated TSA′ species (≈20–23°). The larger twist angle results in a wider opening angle between phosphonate oxygen atoms, thereby allowing water coordination. On the contrary, the twist angle of acetate pendants changes from approximately 22° (Nd) to around 27° (Sm) in the hydrated species and remains unchanged in the non-hydrated TSA′ species (≈25–26°). Similarly, smaller twist angles of the carboxylate pendant arms versus that of the phosphonate arm were found in the solid-state structure of the $[Nd(Hdo3ap)(H_2O)]^-$ complex.[15] The non-hydrated TSA′ Ln^{III}–H_5do3ap complexes have twist angles that are almost the same for both carboxylate and phosphonate pendant arms,[14] thereby confirming that the addition of only one phosphonate group to the dota structure changes the properties of the complexes only slightly. The nitrogen atoms of the macrocycle almost form a regular plane (distances of the nitrogen atoms from the mean plane are ≈0.01 Å). On the contrary, the O_4 plane is more unsymmetrical due to the different character of the pendant arms (differences of ≈0.06 Å for TSA species and ≈0.15 Å for the TSA′ species, respectively). As the radius of the Ln^{III} decreases, the central ions shift from the O_4 plane towards the N_4 base, as observed for Ln^{III} complexes of H_4dota or H_5do3ap.[14,15,19,61] Despite a huge disorder of water solvate molecules found, the high number of water molecules and their localisation close to the O_4 plane point to a strong second-sphere hydration of the complexes, as suggested from the luminescence study on the Eu^{III}–$H_6\mathbf{L}$ complex. Analogous hydration has been observed in lanthanide(III) complexes of H_5do3ap[14,15] in the solid state and in europium(III) complexes of tetraphosphorus acid derivatives of cyclen in solution.[18] The crystal structures of the lanthanide(III) complexes of *trans*-H_6do2a2p confirm again that phosphorus-containing pendant arms are able to enhance the second-sphere hydration, which increases the relaxivity of gadolinium(III) complexes of such ligands.[3,23]

Solution-structural NMR spectroscopic studies of the lanthanide(III) complexes of *trans*-H_6do2a2p: The structures of the $[Ln(\mathbf{L})]^{3-}$ complexes in solution are expected to have strong similarities to those of the corresponding $[Ln(dota)]^-$ and $[Ln(dotp)]^{5-}$ complexes.[24] NMR spectroscopic studies have shown that, due to the rigidity of the tetraaza macrocyclic ring, the $[Ln(dota)]^-$ complexes are present in solution as a mixture of two diastereoisomeric forms that differ in the mutual rotation of the N_4 and O_4 planes, thus giving a square-antiprismatic arrangement (SA, torsion angle $\theta > 35°$, with opposite sign of rotation of the pendant arms (Δ/Λ) and the conformation of the ethylene bridges in the macrocycle ring (δ/λ), represented as the Δλλλλ/Λδδδδ enantiomeric pair) and a twisted-square-antiprismatic arrangement (TSA, torsion angle $\theta < 30°$, with the same sign of rotation leading to the Λλλλλ/Δδδδδ enantiomeric pair).[20] However, the $[Ln(dotp)]^{5-}$ complexes, as well as those of various alkyl- (phosphinates) or alkoxy- (phosphonate monoesters) dotp analogues, occur exclusively in the TSA conformation.[18,21,22] The $[Ln(dota)]^-$ complexes show both enantiomerisation and isomerisation in aqueous solution, whereas the more rigid $[Ln(dotp)]^{5-}$ complexes only display the enantiomerisation process.

To obtain further structural information on the $[Ln(\mathbf{L})]^{3-}$ complexes in solution, ^{1}H and ^{31}P NMR spectra were acquired for the whole lanthanide series. Whereas the C_4 symmetry of the $[Ln(dota)]^-$ and $[Ln(dotp)]^{5-}$ complexes leads to ^{1}H NMR spectra with six signals, and one ^{31}P NMR spectroscopic signal for $[Ln(dotp)]^{5-}$,[20,21] the $[Ln(\mathbf{L})]^{3-}$ complexes with C_2 symmetry show one ^{31}P and twelve ^{1}H NMR spectroscopic resonances.[24] The diamagnetic (Ln = La, Lu, Y) complexes at 298 K exhibit ^{1}H NMR spectra with the expected twelve multiplets (chemical shifts in Table S5 of the Supporting Information), the assignments of which were based upon the previously published studies for the La^{III} and Lu^{III} complexes[24] and g-COSY experiments. The spectra obtained at 298 K are broader than those reported at low temperature (272 K, see ref. [24]), which results from an increased rate of enantiomerisation within the single TSA isomer present in solution for these complexes.[24] The corresponding ^{31}P NMR spectroscopic chemical shifts are in Table S5.

The ^{1}H and ^{31}P NMR spectra of the whole series of paramagnetic $[Ln(\mathbf{L})]^{3-}$ complexes (Ln = Ce–Yb, except Pm and Gd) in solution were also obtained at 298 K. The ^{1}H spectra (Figures 7 and S18, chemical shifts in Table S5 of the Supporting Information) show the expected twelve resonances, which were assigned on the basis of g-COSY spectra for the Ce^{III}–Eu^{III} and Yb^{III} complexes, on the assignment published for the Eu^{III} complex[24] and also by comparison with the shifts of the corresponding protons for the $[Ln(dotp)]^{5-}$ and $[Ln(dota)]^-$ complexes.[20,21] The protons of the complexes are represented in accordance with the labelling in Scheme 1. The corresponding ^{31}P NMR spectra show a single signal (chemical shifts on Table S5). The ^{1}H and

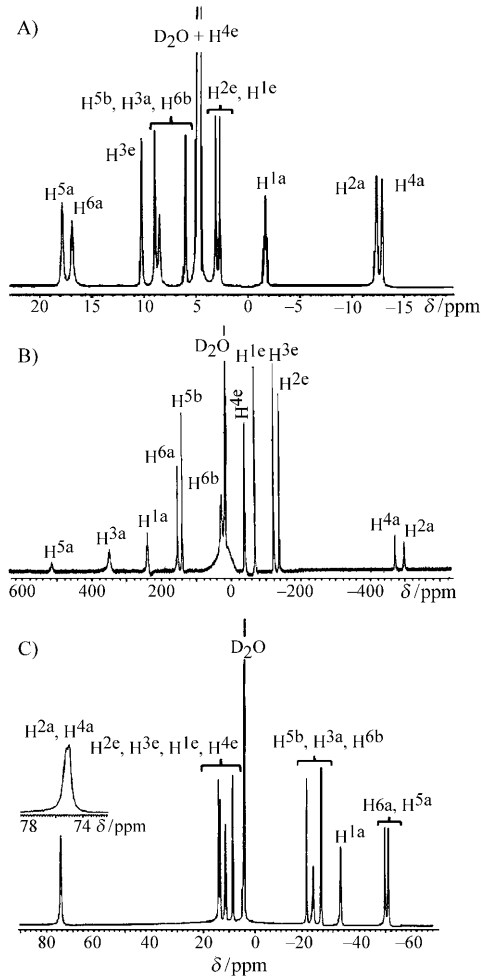

Figure 7. ^{1}H NMR spectra of the $[Ln(\mathbf{L})]^{3-}$ complexes in D_2O (10 mM, 298 K): A) Nd^{III}; B) Tb^{III}; C) Yb^{III} (see inset for expansion of one of the signals).

^{31}P NMR spectroscopic shifts are pH-dependent in the 2.0–8.0 range, which is associated with the protonation of the two Ln^{III}-unbound phosphonate oxygen atoms (see also above). The spectrum of the Eu^{III} complex that shows the presence of two characteristic resonances at about $\delta =$ 24.5 ppm, assigned to two macrocyclic axial protons H^{1a} and H^{3a} (for atom labelling, see Scheme 1) corresponds to the TSA isomer. The spectrum is very similar to that published previously; at 274 K, two sets of twelve resonances were reported for this complex that correspond to 93% TSA isomer and 7% SA isomer, which coalesce at 298 K.[24]

The g-COSY spectra of the Ln^{III} (Ln = Pr, Nd, Sm and Eu) complexes (Figure S19 in the Supporting Information) show eight cross-peaks that correspond to the six geminal proton ($H^{n\,a,e}$, $n = 1$–6) couplings and to two vicinal *trans* couplings (H^{1a},H^{2a} and H^{3a},H^{4a}) within the macrocyclic ring.

For each nucleus studied (*i* means ^{1}H or ^{31}P) in the paramagnetic $[Ln(\mathbf{L})]^{3-}$ complexes, the lanthanide-induced shift (LIS) consists of three contributions,[62] diamagnetic (Δ_i^d), contact (Δ_i^c) and pseudo-contact (or dipolar) (Δ_i^{pc}) [Eq. (6)].

$$LIS_i = \Delta_i^d + \Delta_i^c + \Delta_i^{pc} \quad (6)$$

Upon subtracting the diamagnetic contribution that results from conformational changes, inductive effects and/or direct-field effects (La^{III} was used for Ce^{III}–Eu^{III} and Lu^{III} for Tb^{III}–Yb^{III}), the paramagnetic contribution for nucleus *i* (LIS_i) of the $[Ln(\mathbf{L})]^{3-}$ complexes was obtained and compared with those of the TSA isomer of the corresponding $[Ln(dota)]^{-}$ complexes[20b] and of the $[Ln(dotp)]^{5-}$ complexes[21a] (see Table S6 in the Supporting Information). The contact and pseudo-contact contributions to the observed LIS_i values for the $[Ln(\mathbf{L})]^{3-}$ series of complexes were separated using Equations (7) and (8)[63]

$$LIS_i/ < S_z >_j = F_i + (C_j^D/ < S_z >_j)G_i \quad (7)$$

$$LIS_i/C_j^D = (< S_z >_j/C_j^D)F_i + G_i \quad (8)$$

in which the meaning of the Ln^{III}-dependent parameters ($< S_z >_j$ and C_j^D) and the nucleus-dependent parameters (F_i and G_i) is defined in the Supporting Information.

The plots obtained are illustrated in Figure 8 for the H^{3a} and ^{31}P nuclei according to Equation (7).

The plots for all nuclei studied using Equations (7) and (8) are shown in Figures S20 and S21, respectively, of the Supporting Information. All plots show a break between the early (Ce→Eu) and late (Tb→Yb) lanthanide half-series. Plots according to Equation (8) (Figure S20) show some scatter in the data due to the low contact contribution in the LIS values of the corresponding nuclei. Such breaks have been observed for many series of Ln^{III} complexes,[62,64] including the $[Ln(dota)]^{-}$[20b] and $[Ln(dotp)]^{5-}$ series.[21a] In the

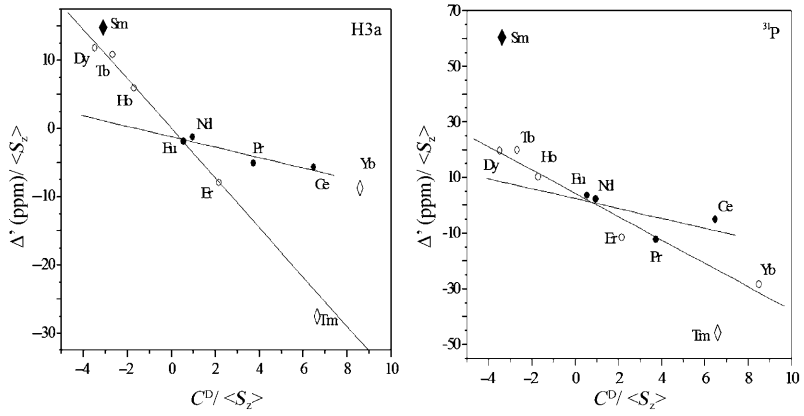

Figure 8. Plots of the H^{3a} and ^{31}P LIS data for separation of contact and pseudo-contact contributions according to Equation (7) for the $[Ln(\mathbf{L})]^{3-}$ complexes.

case of ^{31}P LIS values, the breaks observed for the benzylphosphinate complexes, $[Ln(dotp^{Bn})]^-$ (for structure of H_4dotp^{Bn}, see Scheme 1), which occur in solution as one main isomer (*RRRR* or *SSSS*) at the P atoms, were attributed to a change of water inner-sphere coordination from $q=1$ for (Ce→Nd) to $q=0$ for (Eu→Yb).[27] The phenylphosphinate complexes, $[Ln(dotp^{Ph})]^-$ (for structure of H_4dotp^{Ph}, see Scheme 1), present in solution as a mixture of the six possible isomers with *R* or *S* orientations at the P atoms, did not show such a break and, thus, were considered to be isostructural, with hydration number $q=0$ all along the lanthanide series.[17] However, these conclusions must be taken with care. It has recently been shown for the predominant *RRRR* (*SSSS*) solution isomer of the several Ln^{III} tetraazaphosphinate and tetraazaphosphonate complexes across the lanthanide series, as well as for the $[Ln(dotp)]^{5-}$ complexes, that the positions of the breaks observed in the plots of the ^{17}O water LIS values, which directly reflect the change of inner-sphere water coordination (q value), do not correspond with those observed for the ^{31}P LIS data.[18,22] The breaks of the ^{17}O LIS plots occur at the beginning of the Ln series, which corresponds to a change of $q=1$ for the Ce^{III} complexes to $q=0$ for the rest of the series.[18] The ^{31}P LIS breaks (and also for the other ligand nuclei, for example, ^{1}H) are observed at the middle of the Ln series, thereby indicating a change in both *F* and *G* for the ligand nuclei of these complexes along the Ln series. In the case of the $[Ln(\mathbf{L})]^{3-}$ complexes, the crystal structures described in this work show an abrupt structural change from nona-coordination ($q=1$) for the Ce→Sm, to octa-coordination ($q=0$) for Sm→Yb (in solution, $q=0$ for the $[Gd(\mathbf{L})]^{3-}$[24] and $[Eu(\mathbf{L})]^{3-}$ complexes; see above). They also show a gradual change of the structure of the twisted-square-antiprismatic (TSA) coordination cage, as the distance of the lanthanide(III) ion to the N_4 plane decreases gradually from 1.777 Å for the Ce^{III} complex to 1.584 Å for the Sm^{III} complex, and then remains almost constant in the second half of the lanthanide series (1.507 Å for the Yb^{III} complex). It reflects the movement of the lanthanide(III) ion inside the ligand cavity towards the N_4 plane upon going from La to Sm, after which it remains at a nearly constant position for the rest of the series. Thus, the ^{1}H and ^{31}P LIS breaks may not directly reflect a change of hydration number of the complex but rather the gradual geometrical change of the lanthanide(III) coordination sphere.

To try to answer this question, the structural analysis of the $[Ln(\mathbf{L})]^{3-}$ complexes in solution was pursued through the analysis of the ^{1}H and ^{31}P LIS values. Tables S7 and S8 in the Supporting Information show the values of *F* and *G* and their standard deviations obtained from the linear least-squares analysis of the LIS data using Equations (7) and (8), respectively, by separating the data into two subgroups of lanthanide(III) cations. Sm and Tm atoms were also removed from the fitting procedure.

The analysis of the pseudo-contact shifts to obtain structural information was initiated by assuming structures for the $[Ln(\mathbf{L})]^{3-}$ complexes in solution, thereby allowing the calculation of the geometric factors for the ^{1}H and ^{31}P nuclei. Firstly, for the comparison between the experimental ^{1}H and ^{31}P pseudo-contact LIS values of the $[Ln(\mathbf{L})]^{3-}$ complexes, taken as the experimentally obtained geometric terms of nucleus *i* (G_i values) of Tables S7 and S8, two geometric models were considered. For each model, the atomic coordinates of the ^{1}H and ^{31}P nuclei for the complex with the Ln^{III} fixed at the origin of the system were used as input to the calculation. The atomic coordinates were obtained from those of the crystal structure of the $[Ce(\mathbf{L})(H_2O)]^{3-}$ complex described before, in which the Ce^{III} ion is nona-coordinated by one oxygen of an inner-sphere water molecule, and four macrocyclic nitrogen atoms and four oxygen atoms of the pendant arms, which form two parallel N_4 and O_4 planes with a twisted-square-antiprismatic (TSA) coordination geometry. With $q=1$, this structure is a good starting model for the structure of the complexes of the first half of the Ln series. The other model, used for the second half of the Ln series, was obtained from the crystal structure of the $[Yb(\mathbf{L})]^{3-}$ complex described above, in which the Yb^{III} ion is octa-coordinated by the ligand also with a twisted-square-antiprismatic (TSA) coordination geometry as in the previous case.

The calculated LIS values for the ^{1}H and ^{31}P nuclei of the models were used simultaneously in the calculations, the magnetic symmetry of the complex was assumed to be rhombic and equal weights were used for all LIS values when running the least-squares analysis in the SHIFT ANALYSIS program. Table 9 shows that the agreement between the calculated shifts and experimental G_i values, obtained from Table S7 in the Supporting Information, is quite reasonable for the first part of the Ln series (agreement factor $AF_j=0.286$; for definition, see the Experimental Section) and excellent for the second half ($AF_j=0.052$). Similar results (Table S9) were obtained using the experimental G_i values from Table S8. These results lend support to the con-

Table 9. Comparison of observed[a] and calculated[b] proton pseudo-contact LIS values for the paramagnetic $[Ln(\mathbf{L})]^{3-}$ complexes (standard deviations for the shifts are also shown).

Nucleus	Ce→Eu (−Sm)		Tb→Yb (−Tm)	
	LIS_{exptl} (G_i)	LIS_{calcd}	LIS_{exptl} (G_i)	LIS_{calcd}
H^{1a}	1.55±0.29	0.51±1.34	−1.95±0.09	−1.54±0.61
H^{1e}	1.01±0.26	1.73±0.73	0.63±0.03	0.45±0.40
H^{2a}	2.75±0.06	3.48±1.05	3.78±0.58	3.81±0.58
H^{2e}	1.18±0.16	1.04±0.69	0.90±0.18	0.29±0.39
H^{3a}	−0.76±0.20	−1.14±1.20	−3.62±0.22	−2.69±0.65
H^{3e}	1.13±0.11	0.33±0.69	0.75±0.10	0.10±0.35
H^{4a}	2.15±0.27	2.42±1.07	3.72±0.54	3.57±0.50
H^{4e}	0.15±0.22	0.39±0.69	0.27±0.05	0.41±0.34
H^{5a}	−4.44±0.26	−2.44±1.15	−3.15±0.77	−3.09±0.54
H^{5b}	0.25±0.25	−1.22±0.64	−0.99±0.26	−1.98±0.35
H^{6a}	−2.77±0.10	−1.16±1.09	−2.24±0.14	−2.85±0.65
H^{6b}	0.44±0.09	−0.78±0.71	−0.92±0.11	−1.18±0.35

[a] The observed proton pseudo-contact LIS values are taken as experimentally obtained G_i values of Table S7 [Eq. (7)]. [b] Values calculated using the program SHIFT ANALYSIS and the crystal coordinates obtained for the $[Ce(\mathbf{L})]^{3-}$ and $[Yb(\mathbf{L})]^{3-}$ complexes; $AF_j=0.286$ (Ce–Eu) and $AF_j=0.052$ (Tb–Yb).

clusion that the ^{1}H and ^{31}P LIS breaks do not reflect the change of hydration number of the complexes that occurs at Sm^{III}, but rather the gradual geometrical change of the metal coordination sphere.

Calculations were also performed using the experimental ^{1}H LIS values for the $[Yb(\mathbf{L})]^{3-}$ complex. It was assumed that these LIS values are exclusively of pseudo-contact origin, which is usually a good approximation.[62] Table 10 shows an excellent agreement between the experimental LIS values for the complex and those calculated using the SHIFT ANALYSIS program and the crystal coordinates of the $[Yb(\mathbf{L})]^{3-}$ complex ($AF_j = 0.005$). The magnetic susceptibility tensor (χ) obtained for the complex has rhombic symmetry, with main components $\chi_{xx} = -1402.70$, $\chi_{yy} = 2415.22$ and $\chi_{zz} = -1012.52$, in units of VVk mol^{-1}.

Table 10. Comparison of the observed and calculated proton pseudo-contact LIS values for the $[Yb(\mathbf{L})]^{3-}$ complex.

Nucleus	LIS_{exptl}	LIS_{calcd}
H^{1a}	−36.8	−35.8 ± 3.4
H^{1e}	11.9	7.1 ± 2.2
H^{2a}	70.8	72.7 ± 3.2
H^{2e}	12.5	12.1 ± 2.1
H^{3a}	−20.8	−21.7 ± 3.6
H^{3e}	12.3	12.4 ± 1.9
H^{4a}	70.7	68.1 ± 2.7
H^{4e}	4.5	12.3 ± 1.9
H^{5a}	−52.2	−50.7 ± 2.9
H^{5b}	−20.4	−22.0 ± 1.9
H^{6a}	−51.6	−51.5 ± 3.6
H^{6b}	−28.5	−29.8 ± 1.9

Conclusion

In this paper, we further investigated the complexation properties of *trans*-H_6do2a2p. The structure of the zwitterionic form of the ligand in the solid state exhibits the common features expected for dota-like ligands. The methylphosphonate groups that bear nitrogen atoms are protonated. Dissociation constants of the ligand are similar to those determined previously[24] and the differences can be ascribed to the differences in the supporting electrolyte. Correspondingly, the values of stability constants of the metal complexes are similar; however, richer chemical models for the speciation in solution were determined in this paper. Kinetics of complexation/decomplexation of the Ce^{III} and Eu^{III} complexes was followed at different pH and temperature values. For the Eu^{III} complex, complexation could be followed only in a very narrow range around pH 5.5 and, as expected, proceeds through the "out-of-cage" complex. The rate of dissociation of complexes of these metal ions showed a monotonous dependence on the number of phosphonic acid groups in dota-like ligands. For the Ce^{III} complexes, an increasing number of phosphonic acid groups leads to more inert complexes. For the Eu^{III} complexes, the dependence takes the opposite direction. The most interesting data are those obtained from solid-state structures of the lanthanide(III) complexes. The structures represent one of the most complete published series of complexes with one ligand and lanthanide(III) ions. All complexes are present as twisted-square-antiprismatic isomers. However, a change from nona-coordinated complexes, with one water molecule in the coordination sphere (Ce→Sm), occurs to anhydrous octa-coordinated complexes (Sm→Yb), whereas the central ions move more deeply inside the ligand cavity in the Ce–Sm series and then almost do not move further up to Yb. The experimental ^{1}H NMR spectroscopic pseudo-contact shifts for the Ce–Eu and Tb–Yb series of complexes could be fitted to the crystal structures of the $[Ce(\mathbf{L})]^{3-}$ and $[Yb(\mathbf{L})]^{3-}$ complexes, respectively. The observed breaks in the contact and pseudo-contact separation plots for the ^{1}H and ^{31}P LIS observed at Eu^{III} reflect the gradual geometrical change of the metal coordination sphere rather than the change of hydration number of the complexes that occurs at Sm^{III}. Thus, measurement of the ^{17}O water LIS values is required to study changes of inner-sphere water coordination of the Ln^{III} complexes. In general, this paper presents one of the most complete set of data on Ln^{III}–macrocycle complexes that deals with a correlation between structural parameters obtained from X-ray diffraction studies with those in solution obtained from paramagnetic NMR spectroscopic studies. In addition, these data helped to interpret kinetic data along the lanthanide series.

Experimental Section

General: Chemicals and solvents were of reagent grade and were used without further purification, unless stated otherwise. Deuterium oxide (99.96% D), DCl (35 wt% in D_2O, 99% D) and anhydrous $LnCl_3$ and YCl_3 (Ln = Ce, Pr, Nd, Sm, Eu, Tb, Dy, Ho, Er, Tm, Yb, Lu) were obtained from Aldrich and Alfa Aesar. Deuterated potassium hydroxide solution was freshly prepared just before use. The title ligand, 4,10-bis-(phosphonomethyl)-1,4,7,10-tetraazacyclododecane-1,7-diacetic acid (*trans*-H_6do2a2p, $H_6\mathbf{L}$) in hydrochloride form, was prepared as previously reported.[30a]

Purification of *trans*-H_6do2a2p: The hydrochloride of *trans*-H_6do2a2p (2.5 g) was dissolved in water and purified first using a Dowex 50 column (3.5 × 20 cm, H^+ form) by elution with water and followed by 10% aqueous pyridine. The pyridine fractions were collected and evaporated to dryness. A concentrated aqueous solution of the residue was absorbed using an Amberlite CG50 column (3.5 × 20 cm, H^+ form) and the compound was eluted with water. Early fractions that contained the pure zwitterionic form of the title product were combined and water was evaporated close to dryness, thus yielding a white solid. This solid was filtered, washed with water and dried in air to give the pure compound as $H_6\mathbf{L}\cdot 4H_2O$ (2.1 g). The single crystals of $H_6\mathbf{L}\cdot 4H_2O$ suitable for X-ray analysis were obtained by a slow evaporation of the concentrated aqueous solutions of pure ligand in air.

Synthesis of the lanthanide(III) complexes: Lanthanide(III) complexes were prepared by mixing aqueous solutions of $H_6\mathbf{L}\cdot 4H_2O$ (5 mL, 10 mM) with stoichiometric amounts of the appropriate solid anhydrous $LnCl_3$. The pH of the mixture was adjusted to 8–9 with aqueous KOH and the solutions were heated (50 °C) for 3 h with continuous re-adjustment of the pH to 8. After this time, the reaction mixture was allowed to stand at room temperature for 18 h and then filtered through a SEP-PAK C_{18}-car-

tridge (to remove any free Ln^{III}). Then the pH of the filtered solution was lowered to 3–5 with diluted aqueous HCl (0.1 M) and the solution volume was reduced to 2 mL in vacuum. Single crystals suitable for X-ray analysis were obtained by a slow vapour diffusion of a *i*PrOH/EtOH mixture (1:1) into concentrated aqueous solutions of the corresponding Ln^{III} complexes, over a period of 3–4 months.

X-ray crystallographic analysis: A selected crystal of $H_6\mathbf{L}\cdot 4H_2O$ was mounted on a glass fibre in random orientation using silicone fat. Diffraction data were collected with graphite-monochromatised $Mo_{K\alpha}$ radiation using an Enraf–Nonius KappaCCD diffractometer at 150(1) K (Cryostream Cooler, Oxford Cryosystem) and analysed using the HKL DENZO program package. Cell parameters were determined from all data by using the same program package.[65] The structure was solved by direct methods and refined by full-matrix least-squares techniques (SIR92[66] and SHELXL97[67]). The scattering factors used for neutral atoms were included in SHELXL97 program. Selected crystals of the lanthanide(III) complexes were quickly transferred into Fluorolub oil (Merck) and centred. Diffraction data were collected with graphite-monochromatised $Mo_{K\alpha}$ radiation ($\lambda = 0.71073$ Å). Crystallographic data for the trivalent Ce, Nd, Sm, Eu, Tb, Dy, Er and Yb complexes were collected using a Bruker AXS APEX CCD area detector diffractometer at 150(1) K (Cryostream Cooler, Oxford Cryosystem) in the ω and ϕ scans mode. A semi-empirical absorption correction was carried out using SADABS.[68] Data collection, cell refinement and data reduction were done with the SMART and SAINT programs.[69] The structures were solved by direct methods using SIR97[70] and refined by full-matrix least-squares methods with SHELXL97.[67] Molecular graphics were prepared using PLATON98.[71]

In the structure of $H_6\mathbf{L}\cdot 4H_2O$, all non-hydrogen atoms were refined anisotropically; all hydrogen atoms were localised in the difference map of the electronic density; however, in the final cycles, they were fixed in theoretical (C–H) or original (N–H, O–H) positions using $U(H) = 1.2\,U(X)$.

In the isostructural compounds $K[Ln(H_2\mathbf{L})(H_2O)]\cdot KCl\cdot 5H_2O$ (Ln = Ce and Nd), the non-hydrogen atoms were refined with anisotropic thermal parameters; in the case of the Nd structure, thermal parameters of one carbon atom were restrained using the ISOR command to keep them positive. Hydrogen atoms that belonged to the complex molecule could be localised in the difference map of the electronic density (even the ones attached to phosphonate oxygen atoms); however, in the final cycles, they were fixed in theoretical (C–H) or original (O–H) positions using $U(H) = 1.2\,U(X)$. In the structures, there remained three large difference maxima. Two of them, close to oxygen atoms of the complex molecules, were interpreted as potassium(I) counterions, and the third one that lay in the relatively free space was attributed to a chloride anion. The potassium(I) ions connect the neighbouring complex molecules into zigzag chains through relatively long coordination bonds (d(O–K) ≈ 2.6–2.9 Å). Other electronic maxima were attributed to water solvate molecules, some of them with half-occupancy. The hydrogen atoms that belonged to most of the water molecules were located in the electronic density map, and were fixed in original positions using $U(H) = 1.2\,U(O)$.

In the structure of $K_3[Sm(H_2\mathbf{L})(H_2O)][Sm(H\mathbf{L})(H_2O)]\cdot KCl\cdot 16H_2O$, two complex molecules were clearly identified in the asymmetric unit. The five largest electronic maxima were treated as four potassium(I) counterions (those close to the oxygen atoms of the complex molecules) and one chloride anion. The potassium(I) ions connect the neighbouring complex molecules into a two-dimensional coordination polymer and form warped plane through relatively long coordination bonds (d(O–K) ≈ 2.6–2.9 Å). Other electronic maxima were attributed to water solvate molecules, some of them with half-occupancy. The non-hydrogen atoms were refined with anisotropic thermal parameters; thermal parameters of two carbon atoms and two oxygen atoms of water solvate molecules were restrained using the ISOR command to keep them positive. All hydrogen atoms (including those belonging to the water solvate molecules) were located in the electronic density map. In the final cycles, they and were fixed in theoretical (C–H) or original (O–H) positions using $U(H) = 1.2\,U(X)$.

In the isostructural series $K_2[Ln(H\mathbf{L})]\cdot 6.5H_2O$ (Ln = Sm, Tb, Dy, Er and Yb), the molecule of the complex possesses a crystallographic two-fold symmetry. Thus, only one half of the macrocyclic skeleton, one pendant phosphonate arm and one acetate arm form the asymmetric unit, with the central metal ion laying on the special (half-occupied) position. The hydrogen atoms that belong to the complex molecule could be localised in the electronic density difference map; the one associated with the phosphonate pendant arm lies on the special position with half-occupancy and connects neighbouring complex molecules into infinite chains. Such a motif results in a formally mono-protonated complex molecule. In the structure, the three largest difference maxima were attributed to two potassium(I) counterions (one maximum lay on the special position with half-occupancy to one ion, and the remaining two maxima were attributed to the disordered second potassium(I) ion. The potassium(I) ions connect the chains of the complex molecules into double chains through relatively long coordination bonds (d(O–K) ≈ 2.6–3.0 Å). Other electronic maxima were attributed to water solvate molecules, some of them with half or quarter occupancy to obtain reliable thermal parameters. Some hydrogen atoms that belonged to the water molecules were also located in the electronic density map. All non-hydrogen atoms were refined with anisotropic thermal parameters, and the hydrogen atoms were fixed in theoretical (C–H) or original (O–H) positions using a riding model with $U(H) = 1.2\,U(X)$.

The close similarity of crystallographic parameters of the Eu^{III} complex points to the isostructurality of this compound with the previous group and, thus, the formula $K_2[Eu(H\mathbf{L})]\cdot 6.5H_2O$ was suggested. However, a brief inspection of the crystal data revealed a huge disorder in the complex molecule. The complex molecule lies on the crystallographic two-fold axis (as in the case of the whole isostructural series), and was best refined as a superposition of two overlying enantiomeric molecules (with refined occupancies of approximately 60:40%), which only have the central ion and the pivot atoms of the pendant arms in common (Figure S17 in the Supporting Information). The remaining maxima of electronic density lay very close to each other, thereby suggesting a disorder and non-full occupancy of the potassium(I) cations and the solvate molecules. Therefore, a squeeze of the residual electronic density was applied using PLATON98.[71] After squeezing, there were still two relatively high maxima left; two maximal peaks (very close to each other) were assigned as a potassium(I) counterion disordered over two positions and had reliable thermal parameters. The other two maxima were attributed to partially occupied water solvate molecules. As anisotropic refinement of non-hydrogen atoms led to several non-positive definites, the ISOR constraint was applied. Hydrogen atoms attached to carbon atoms were fixed using a riding model with $U(H) = 1.2\,U(C)$. Although the calculated lengths and bond angles are loaded with principally high error, their values are very reasonable and fall into the trends of the values found in the other structures (see below).

All complexes crystallised in centrosymmetric groups; in all structures, except that of the Eu^{III} complex, the Λλλλλ complex unit with clockwise numbering of the macrocycle was defined as the independent unit to obtain directly comparable structural parameters (Table 8). In the case of the Eu^{III} complex, the Λλλλλ torsion was chosen for the more abundant part, and the less abundant one was chosen as Δδδδδ. A summary of the experimental crystallographic data is given in Table S10 of the Supporting Information. CCDC-764613, 764614, 764615, 764616, 764617, 764618, 764619, 764620, 764621 and 764622 contain the supplementary crystallographic data for this paper. These data can be obtained free of charge from The Cambridge Crystallographic Data Centre via www.ccdc.cam.ac.uk/data_request/cif.

Potentiometric titrations: The stock/titration solutions of aqueous HCl (≈0.03 M), NMe_4OH (≈0.2 M) and metal chlorides or nitrates used were the same as in previous studies.[36,39] Titrations were carried out in a vessel equipped with a thermostat at (25.0 ± 0.1) °C, at ionic strength I = 0.1 M (NMe_4Cl) and in the presence of extra HCl in the $-\log[H^+]$ range 1.7–11.9 (or until precipitation of a metal hydroxide) using a PHM 240 pH meter, a 2 mL ABU 900 automatic piston burette and a GK 2401B combined electrode (all Radiometer, Denmark). The initial volume was

5 mL and the concentration of the ligand was approximately 0.004 M. An inert atmosphere was ensured by constant passage of argon saturated with the solvent vapour. For the ligand, five parallel titrations were carried out; each titration consisted of about 40 points. Titrations with metal ions were performed at metal-to-ligand molar ratios of 1:1 and 2:1 (at least three parallel titrations, about 40 points each). In the case of lanthanide(III) ions, the complexation was too slow for conventional titration and, therefore, the "out-of-cell" method was used. Each out-of-cell titration consisted of 25 points (solution volume 1 mL) in the $-\log[H^+]$ range 1.8–6.0 (at least two parallel titrations for each 1:1 and 2:1 metal-to-ligand ratio). Equilibrium was reached after 3 weeks at room temperature. The constants determined by this technique showed higher standard deviations due to less precise measurements and a smaller number of experimental points.

The constants (with standard deviations) were calculated with the program OPIUM.[72] The program minimises the criterion of the generalised least-squares method using the calibration function $E=E_0+S\times\log[H^+]+j_1\times[H^+]+j_2\times(K_w/[H^+])$, in which the additive term E_0 contains the standard potentials of the electrodes used and contributions of inert ions to the liquid-junction potential, S corresponds to the Nernstian slope (the value of which should be close to the theoretical value) and the $j_1\times[H^+]$ and $j_2\times[OH^-]=j_2\times(K_w/[H^+])$ terms are the contributions of the H^+ and OH^- ions to the liquid-junction potential. It is clear that j_1 and j_2 cause deviation from a linear dependence of E on pH only in strongly acidic and strongly alkaline solutions. The calibration parameters were determined from titration of the standard HCl with the standard NMe_4OH before each ligand or ligand–metal titration to give a pair of calibration/titration values, which was used for calculations of the constants. The overall protonation constants β_n are concentration constants, defined by $\beta_n=[H_n\mathbf{L}]/([H]^n\times[\mathbf{L}])$. The stability constants are defined by $\beta_{hlm}=[H_h\mathbf{L}_l M_m]/([H]^h\times[\mathbf{L}]^l\times[M]^m)$. The water ion product pK_w (13.81) and stability constants of the $M^{II/III}$–OH^- systems included into the calculations were taken from ref. [73]. The highest protonation constant cannot be measured by potentiometry (it is too high and therefore out of the range in which the glass electrode can be reliably used); it was therefore calculated from changes of δ_P of the phosphonate groups in the strongly alkaline solutions (see below). In the final calculation of the protonation constants, a simultaneous fitting of the NMR spectroscopic and potentiometric data was used.

NMR spectroscopic experiments: The quantitative $^{31}P\{^1H\}$ NMR spectroscopic titration experiments for the determination of the first protonation constant of $H_6\mathbf{L}$ ($-\log[H^+]$ range 11.5–13.6, about 15 points) were carried out under conditions close to the potentiometric titrations (aqueous solution, $I=0.1$ M (NMe_4(Cl,OH)), 25.0 °C, ligand concentration ≈ 0.004 M) according to the IUPAC recommendation.[74] The measurements over $-\log[H^+]=13$ were done without control of the ionic strength. The NMR spectra were recorded using a Varian UnityPlus 400 spectrometer at 169 MHz with an external standard (85% aqueous H_3PO_4); a coaxial capillary with D_2O was used for the lock. The solution $-\log[H^+]$ was adjusted with aqueous NMe_4OH or HCl solutions.

The solutions (2×10^{-3} M) used for the NMR spectroscopic titration measurements over the whole pH range were made using D_2O as solvent and the pD value was raised to near 13 by adding CO_2-free KOD. These solutions were then titrated to low pD with DCl/D_2O and ^1H and ^{31}P NMR spectra were recorded as a function of pD. The pD values were measured directly in the NMR spectroscopy tube with a combined microelectrode (Mettler–Toledo U402-M3-S7/200) and transferred to pH using pH = pD − 0.40.[75] The microelectrode was calibrated with standard buffer solutions (pH 4.01, 7.00, 9.21). The NMR spectra were recorded using Varian Inova-300 NMR spectrometer (^1H 300 MHz; ^{31}P 121.5 MHz) with the internal reference (2-trimethylsilyl)propionic acid ($\delta_H=0.0$ ppm), and external reference 85% aqueous H_3PO_4 solution ($\delta_P=0.0$ ppm) for ^1H and ^{31}P, respectively.

NMR spectra of the Ln^{III}–$H_6\mathbf{L}$ complexes were recorded using Varian VNMRS-600 (^1H 600.14 MHz), Varian Unity-500 (^1H 499.82 MHz), or Varian Inova-300 NMR spectrometers (^1H 300 MHz; ^{31}P 121.5 MHz). The NMR spectra were recorded in D_2O (min 99.96% D, Aldrich) and the $^1H/^{31}P$ NMR chemical shifts (δ) are given in ppm relative to (2-trimethylsilyl)propionic acid (TSP, internal reference; $\delta_H=0.0$ ppm), and to 85% aqueous H_3PO_4 solution (external reference; $\delta_P=0.0$), respectively.

The Ln^{III}–$H_6\mathbf{L}$ solutions for the NMR spectroscopic pH titration were prepared as follows. A solution of $H_6\mathbf{L}$ in D_2O (10 mM) was neutralised with a freshly prepared solution KOD/D_2O (≈ 1.5 M) and a stoichiometric amount of anhydrous $LnCl_3$ dissolved in D_2O (≈ 0.2 mL) was added. The pD of the reaction mixture was continuously measured until stabilisation and then the pD was slowly increased to about 13 by adding the KOD/D_2O solution. These solutions were then titrated to low pD with DCl/D_2O and ^1H and ^{31}P NMR spectra were recorded as a function of pD. The pD measurements for these NMR spectroscopic studies were performed using an ORION SA 720 potentiometer directly in the NMR spectroscopy tube with a combination microelectrode U402-M3-S7/200 (Mettler–Toledo) calibrated at (21 ± 0.5) °C with three standard buffers (pH 4.01, 7.00 and 9.21). Before plotting the data, the pD values of these D_2O solutions was converted to the pH values using the deuterium isotopic correction pH = pD − 0.40.[75] The protonation constants of the free ligand and of its lanthanide(III) complexes were calculated with the HYPNMR program using the δ_P of the complexes at the different pH.[76]

The 10 mM solutions of the $[Ln(\mathbf{L})]^{3-}$ complexes (Ln = La–Lu and Y, except Pm and Gd) were used to obtain 1D spectra, whereas only some of them (Ln = La, Ce, Pr, Nd, Sm, Eu, Lu and Y) were used for 2D g-COSY measurements. These studies were performed at pH ≈ 10 and T = 298 K using Varian Unity-500 or Varian Inova-300 spectrometers. The paramagnetic contributions to the lanthanide-induced shifts (LIS) and relaxation rates were determined as previously described.[21a] The LIS data were analysed with the SHIFT ANALYSIS program developed by Forsberg,[77] in which no assumption is made about the magnetic symmetry of the complex and which uses as input data the Cartesian coordinates of the complexes with the lanthanide(III) ion at the origin. The experimental pseudo-contact LIS geometric factors (G) were fitted to calculated values for various isomeric structures using the components of the susceptibility tensor as adjustable parameters; averaging of G values of symmetry-related resonances was not carried out prior to the comparison with the experimental values. The agreement between the observed and calculated values was evaluated using Hamilton's crystallographic agreement factor,[78] defined as $AF_j=[\Sigma_i(\delta_{ij}^{exptl}-\delta_{ij}^{calcd})^2]/[\Sigma_i(\delta_{ij}^{exptl})^2]^{1/2}$, in which δ_{ij}^{exptl} and δ_{ij}^{calcd} represent the observed and calculated shift values of a nucleus i in a given Ln^{III} complex j, respectively.

Kinetic measurements: The experimental methodology for the kinetic studies on the $[Ln(\mathbf{L})]^{3-}$ complexes was the same as described elsewhere.[36,52,53] All kinetic measurements were carried out using a UV 2 (Pye Unicam) double-beam spectrometer, an HP-8453A (Hewlett–Packard) diode array spectrophotometer and/or an Aminco Bowman AB2 fluorimeter. Luminescence spectra/lifetimes of the $[Eu(\mathbf{L})]^{3-}$ complexes dissolved in H_2O or D_2O were measured using an Aminco Bowman AB2 fluorimeter.

The experimental methodology for the time-resolved luminescence spectroscopy (TRLS) experiments and their application in kinetic studies (the Eu^{III} complex) were described elsewhere.[52,53] The time dependence of the number of coordinated water molecules, q, determined by TRLS was fitted using Equation (9) to afford the value of the rate constant k^*.

$$q_t = e^{-kt}[q_{t=0}(\mathrm{EuL}^*) - q_{t=\infty}(\mathrm{EuL})] + q_{t=\infty}(\mathrm{EuL}) \qquad (10)$$

The formation kinetics were measured at pH 5.5, $I=0.1$ M KCl, temperature range 20–40 °C and $c_L=c_{Eu}=0.0005$ M. The luminescence lifetimes were measured at 594 nm ($^5D_0\rightarrow{}^7F_1$ transition). The second-order rate constant, $^tk_2$, was calculated from UV/Vis spectroscopic data obtained analogously to the published methodology.[58]

The acid-assisted decomplexation reaction of the $[Ln(\mathbf{L})]^{3-}$ complexes was performed at ionic strength $I=3.0$ M (H,Na)ClO_4 ($c_{LnL}\approx(1–2.5)\times10^{-3}$ M) and $[H^+]=0.05–3.00$ M. The progress of the reaction was followed by a change of emission spectra (Eu: $\lambda_{exc}=394$ nm; Gd: $\lambda_{exc}=272$ nm; Tb: $\lambda_{exc}=368$ nm; changes followed over the whole emission spectra) or absorption spectra at the CT band (Ce: $\lambda=310$ nm). The activation pa-

rameters for the Ln^{III} complex dissociation were obtained from the temperature dependence in the range 25–60 °C. The data from kinetic experiments were processed by non-linear regression using EXCEL, HP and/or PROK-II[79] software with identical results and the measured values of the analytical signal were corrected for a background signal. Changes of the hydration number, q, were followed as above.

UV/Vis spectra of the Eu^{III} complex: The $[Eu(\mathbf{L})]^{3-}$ complex was prepared by mixing ligand hydrate (0.100 g) with an aqueous solution of $EuCl_3$ (1 equiv), and aqueous KOH solution was added stepwise over 2 h to reach a constant pH of 6.5. To ensure the full complexation, the solution was stirred overnight. Then, the pH was adjusted to 7.5 and the concentration of the complex to 20 mM. UV/Vis measurements were carried out using a Perkin–Elmer Lambda 19 spectrometer in the 577–581 nm region with data steps of 0.01 nm. The temperature was maintained constant by using thermostatable cells with an optical length of 10 cm. The quality of the results was increased by recording a large number of spectra (40 spectra for 298 K, 80 spectra for 343 K).

Supporting Information available: Experimental detailed data with Figures S1–S21 on NMR pH titrations and protonation sequence of $(\mathbf{L})^{6-}$, species distribution diagrams of the Cu^{II}–$H_6\mathbf{L}$ and Ho^{III}–$H_6\mathbf{L}$ from potentiometry, ^{31}P NMR titration of the $[Pr(\mathbf{L})]^{3-}$ and $[Yb(\mathbf{L})]^{3-}$ complexes, absorption spectrum of Eu^{III}–$H_6\mathbf{L}$, absorption spectra during dissociation of the $[Ce(H_2O)(\mathbf{L})]^{3-}$ complexes in acidic medium, luminescence emission spectra for the Eu^{III}–$H_6\mathbf{L}$ complex formation, number coordinated water molecules during the formation of the $[Eu(\mathbf{L})]^{3-}$ complex followed by TRLS, dependence of pseudo-first order rate constant of the acid-assisted dissociation of $[Eu(\mathbf{L})]^{3-}$, definition of the geometric parameters of Ln^{III} complexes with dota-like ligands, crystal packing of $K[Ce(H_2\mathbf{L})(H_2O)]\cdot KCl\cdot 5H_2O$, molecular structures of the $[Sm(H_2\mathbf{L})(H_2O)]^-$ and $[Sm(H\mathbf{L})(H_2O)]^{2-}$ anions found in the structure of $K_3[Sm(H_2\mathbf{L})(H_2O)][Sm(H\mathbf{L})(H_2O)]\cdot KCl\cdot 16H_2O$ and crystal packing in the structure, crystal packing of $K_2[Dy(H\mathbf{L})]\cdot 6.5H_2O$, disordered structure found in the structure of $K_2[Eu(H\mathbf{L})]\cdot 6.5H_2O$, ^1H 1D and g-COSY NMR spectra of paramagnetic $[Ln(\mathbf{L})]^{3-}$ complexes, plots of the proton LIS data for separation of contact and pseudo-contact contributions for the $[Ln(\mathbf{L})]^{3-}$ complexes, protonisation scheme of $H_6\mathbf{L}$, tables with selected bond lengths and angles of the *trans*-H_6do2a2p molecule and hydrogen-bond geometries in the solid-state structure of $H_6\mathbf{L}\cdot 4H_2O$, overall stability constants ($\log\beta_{hlm}$) of complexes of some divalent and trivalent metal ions with $H_6\mathbf{L}$, average hydration number of complex species present in reaction mixtures in the Eu^{III}–$H_6\mathbf{L}$ system at pH values of 4, 5 and 6 after 24 h, ^1H and ^{31}P NMR spectroscopic chemical shifts and LIS values of the $[Ln(\mathbf{L})]^{3-}$and comparison with the values for the equivalent nuclei in the TSA isomer of the corresponding $[Ln(dota)]^-$ and $[Ln(dotp)]^{5-}$ complexes, separation of contact and pseudo-contact contributions to the observed LIS values in the $[Ln(\mathbf{L})]^{3-}$ complexes, comparison of observed and calculated proton pseudo-contact LIS values for the paramagnetic $[Ln(\mathbf{L})]^{3-}$ complexes and experimental crystallographic data for $H_6\mathbf{L}$ and for its lanthanide(III) complexes; text on theory of separation of contact and pseudo-contact contributions to LIS of complexes.

Acknowledgements

This work was financially supported by the Fundação para a Ciência e a Tecnologia (FCT), Portugal (project POCTI/CBO/35859/99 (for I.S.), PTDC/QUI/70063/2006 (for C.F.G.C.G.), and post-doctoral grants SFRH/BD/19168/2004 (to S.L.) and SFRH/BPD/35005/2007 (to G.A.P.)), FEDER, the Grant Agency of the Czech Republic (grant no. 203/09/1056 (P.H.)), the Czech Academy of Sciences (grant no. KAN201110651 (P.H.)), the Ministry of Education, Youth and Sport of the Czech Republic (grant nos. MSM0021620857 (P.H.), LC06035 and ME09065 (P.L.)), the Gabinete de Relações Internacionais da Ciência e Ensino Superior (GRICES) of Portugal (Grices/AS CR 2006 (P.H. and I.S.)) and the Institut National du Cancer and La Ligue Contre le Cancer, France (É.T.). The Varian VNMRS 600 NMR spectrometer in Coimbra was purchased with the support of the Programa Nacional de Reequipamento Científico of FCT, Portugal, contract REDE/1517/RMN/2005, as part of RNRMN (Rede Nacional de RMN). The authors thank to Dr. Ivana Císařová for collection of the X-ray data of the ligand crystal and Radek Ševčik for technical assistance. This work was carried out within the framework of the COST D38 and BM607 Actions and EU-FP6 "Network of Excellence" DiMI (grant no. LSHB-2005-512146) project.

[1] E. Brücher, *Top. Curr. Chem.* **2002**, *221*, 103–122.
[2] R. Delgado, V. Félix, L. M. P. Lima, D. W. Price, *Dalton Trans.* **2007**, 2734–2745.
[3] P. Hermann, J. Kotek, V. Kubíček, I. Lukeš, *Dalton Trans.* **2008**, 3027–3047.
[4] a) C. P. Montgomery, B. S. Murray, E. J. New, R. Pal, D. Parker, *Acc. Chem. Res.* **2009**, *42*, 925–937; b) C. M. G. dos Santos, A. J. Harte, S. J. Quinn, T. Gunnlaugsson, *Coord. Chem. Rev.* **2008**, *252*, 2512–2527.
[5] a) L. R. Dick, C. F. G. C. Geraldes, A. D. Sherry, C. W. Gray, D. M. Gray, *Biochemistry* **1989**, *28*, 7896–7904; b) P. H. J. Keizers, A. Saragliadis, Y. Hiruma, M. Overhand, M. Ubbink, *J. Am. Chem. Soc.* **2008**, *130*, 14802–14812.
[6] *The Chemistry of Contrast Agents in Medical Magnetic Resonance Imaging* (Eds.: A. E. Merbach, E. Tóth), Wiley, New York, **2001**.
[7] a) S. Aime, M. Botta, E. Terreno, *Adv. Inorg. Chem.* **2005**, *57*, 173–237; b) S. Aime, S. Geninatti Crich, E. Gianolio, G. B. Giovenzana, L. Tei, E. Terreno, *Coord. Chem. Rev.* **2006**, *250*, 1562–1579.
[8] P. Caravan, *Chem. Soc. Rev.* **2006**, *35*, 512–523.
[9] *Contrast Agents in Magnetic Resonance Imaging, Vol. 221* (Ed.: W. Krause), Springer, Heidelberg, **2002**.
[10] C. F. G. C. Geraldes, S. Laurent, *Contrast Media Mol. Imag.* **2009**, *4*, 1–23.
[11] a) D. C. Buster, M. M. C. A. Castro, C. F. G. C. Geraldes, C. R. Malloy, A. D. Sherry, T. C. Siemers, *Magn. Reson. Med.* **1990**, *15*, 25–32; b) N. Bansal, M. J. Germann, V. Seshan, G. T. Shires III, C. R. Malloy, A. D. Sherry, *Biochemistry* **1993**, *32*, 5638–5643; c) J. Ren, A. D. Sherry, *Inorg. Chim. Acta* **1996**, *246*, 331–341.
[12] a) S. Liu, *Adv. Drug Delivery Rev.* **2008**, *60*, 1347–1370; b) M. W. Brechbiel, *Eur. J. Nucl. Med. Mol. Imaging* **2008**, *52*, 166–173; c) S. P. Fricker, *Chem. Soc. Rev.* **2006**, *35*, 524–533; d) "Radiolanthanides in Nuclear Medicine": F. Rösch and E. Forssell-Aronsson in *Metal Ions In Biological Systems, Vol. 42* (Eds.: A. Siegel, H. Siegel), Marcel Dekker, New York, **2004**, pp. 77–178.
[13] F. Avecilla, J. A. Peters, C. F. G. C Geraldes, *Eur. J. Inorg. Chem.* **2003**, 4179–4186.
[14] J. Rudovský, P. Cígler, J. Kotek, P. Hermann, P. Vojtíšek, I. Lukeš, J. A. Peters, L. V. Elst, R. N. Muller, *Chem. Eur. J.* **2005**, *11*, 2373–2384.
[15] P. Vojtíšek, P. Cígler, J. Kotek, J. Rudovský, P. Hermann, I. Lukeš, *Inorg. Chem.* **2005**, *44*, 5591–5599.
[16] S. Aime, A. S. Batsanov, M. Botta, J. A. K. Howard, D. Parker, K. Senanayake, G. Williams, *Inorg. Chem.* **1994**, *33*, 4696–4706.
[17] J. Rohovec, P. Vojtíšek, P. Hermann, J. Mosinger, Z. Žák, I. Lukeš, *J. Chem. Soc. Dalton Trans.* **1999**, 3585–3592.
[18] Z. Kotková, G. A. Pereira, K. Djanashvili, J. Kotek, J. Rudovský, P. Hermann, L. V. Elst, R. N. Muller, C. F. G. C. Geraldes, I. Lukeš, J. A. Peters, *Eur. J. Inorg. Chem.* **2009**, 119–136.
[19] J. Kotek, J. Rudovský, P. Hermann, I. Lukeš, *Inorg. Chem.* **2006**, *45*, 3097–3102.
[20] a) S. Aime, M. Botta, M. Fasano, M. P. M. Marques, C. F. G. C. Geraldes, D. Pubanz, A. E. Merbach, *Inorg. Chem.* **1997**, *36*, 2059–2068; b) M. P. M. Marques, C. F. G. C. Geraldes, A. D. Sherry, A. E. Merbach, H. Powell, D. Pubanz, S. Aime, M. Botta, *J. Alloys Compnd.* **1995**, *225*, 303–307; c) V. Jacques, J. F. Desreux, *Inorg. Chem.* **1994**, *33*, 4048–4053; d) S. Aime, M. Botta, G. Ermondi, *Inorg. Chem.* **1992**, *31*, 4291–4299; e) J. F. Desreux, *Inorg. Chem.* **1980**, *19*, 1319–1324.
[21] a) C. F. G. C. Geraldes, A. D. Sherry, G. E. Kiefer, *J. Magn. Reson.* **1992**, *97*, 290–304; b) J. Ren, A. D. Sherry, *J. Magn. Reson.* **1996**,

B111, 178–182; c) A. D. Sherry, C. F. G. C. Geraldes, W. P. Cacheris, *Inorg. Chim. Acta* **1987**, *139*, 137–139.
[22] G. A. Pereira, L. Ball, A. D. Sherry, J. A. Peters, C. F. G. C. Geraldes, *Helv. Chim. Acta* **2009**, *92*, 2532–2551.
[23] a) J. Rudovský, J. Kotek, P. Hermann, I. Lukeš, V. Mainero, S. Aime, *Org. Biomol. Chem.* **2005**, *3*, 112–117; b) J. Rudovský, M. Botta, P. Hermann, A. Koridze, S. Aime, *Dalton Trans.* **2006**, 2323–2333; c) P. Lebdušková, P. Hermann, L. Helm, É. Tóth, J. Kotek, K. Binnemans, J. Rudovský, I. Lukeš, A. E. Merbach, *Dalton Trans.* **2007**, 493–501.
[24] a) F. K. Kálmán, Z. Baranyai, I. Tóth, I. Bányai, R. Király, E. Brücher, S. Aime, X. Sun, A. D. Sherry, Z. Kovács, *Inorg. Chem.* **2008**, *47*, 3851–3862; b) F. K. Kálmán, PhD Thesis, University of Debrecen (Hungary), **2007**.
[25] M. P. Campello, M. Balbina, I. Santos, P. Lubal, R. Ševčík, R. Ševčíková, *Helv. Chim. Acta* **2009**, *92*, 2398–2413.
[26] A. Harrison, C. A. Walker, K. A. Pereira, D. Parker, L. Royle, K. Pulukkody, T. J. Norman, *Magn. Reson. Imaging* **1993**, *11*, 761–770.
[27] S. Aime, A. S. Batsanov, M. Botta, R. S. Dickins, S. Faulkner, C. E. Foster, A. Harrison, J. A. K. Howard, J. M. Moloney, T. J. Norman, D. Parker, L. Royle, J. A. G. Williams, *J. Chem. Soc. Dalton Trans.* **1997**, 3623–3636.
[28] C. F. G. C. Geraldes, A. D. Sherry, I. Lázár, A. Miseta, P. Bogner, E. Berenyi, B. Sumegi, G. E. Kiefer, K. McMillan, F. Maton, R. N. Muller, *Magn. Reson. Med.* **1993**, *30*, 696–703.
[29] F. C. Alves, P. Donato, A. D. Sherry, A. Zaheer, S. Zhang, A. J. M. Lubag, M. E. Merritt, R. E. Lenkisnski, J. V. Frangioni, M. Neves, M. I. M. Prata, A. C. Santos, J. J. P. de Lima, C. F. G. C. Geraldes, *Invest. Radiol.* **2003**, *38*, 750–760.
[30] a) M. P. Campello, F. Marques, L. Gano, S. Lacerda, I. Santos, *Radiochim. Acta* **2007**, *95*, 329–334; b) F. Marques, L. Gano, M. P. Campello, S. Lacerda, I. Santos, *Radiochim. Acta* **2007**, *95*, 335–341; c) L. Gano, F. Marques, M. P. Campello, M. Balbina, S. Lacerda, I. Santos, *Q. J. Nucl. Med. Mol. Imaging* **2007**, *51*, 6–15.
[31] M. Försterová, Z. Jandurová, F. Marques, L. Gano, P. Lubal, J. Vaněk, P. Hermann, I. Santos, *J. Inorg. Biochem.* **2008**, *102*, 1531–1540.
[32] M. Försterová, M. Petřík, A. Lázničková, M. Lázníček, P. Hermann, I. Lukeš, F. Melichar, *Appl. Radiat. Isot.* **2009**, *67*, 21–29.
[33] S. Lacerda, F. Marques, P. Campello, L. Gano, V. Kubíček, P. Hermann, I. Santos, *J. Labelled Compd. Radiopharm.* **2010**, *53*, 36–43.
[34] a) F. Marques, K. P. Guerra, L. Gano, J. Costa, M. P. Campello, L. M. P. Lima, R. Delgado, I. Santos, *J. Biol. Inorg. Chem.* **2004**, *9*, 859–872; b) F. Marques, L. Gano, M. P. Campello, S. Lacerda, I. Santos, L. M. P. Lima, J. Costa, P. Antunes, R. Delgado, *J. Inorg. Biochem.* **2006**, *100*, 270–280.
[35] I. Lukeš, J. Kotek, P. Vojtíšek, P. Hermann, *Coord. Chem. Rev.* **2001**, *216–217*, 287–312.
[36] P. Táborský, P. Lubal, J. Havel, J. Kotek, J. Rudovský, P. Hermann, I. Lukeš, *Collect. Czech. Chem. Commun.* **2005**, *70*, 1909–1942.
[37] I. Lázár, C. H. Duane, W. Kim, C. E. Kiefer, A. D. Sherry, *Inorg. Chem.* **1992**, *31*, 4422–4424.
[38] S. Aime, A. Barge, J. I. Bruce, M. Botta, J. A. K. Howard, J. M. Moloney, D. Parker, *J. Am. Chem. Soc.* **1999**, *121*, 5762–5771.
[39] M. Försterová, I. Svobodová, P. Lubal, P. Táborský, J. Kotek, P. Hermann, I. Lukeš, *Dalton Trans.* **2007**, 535–549.
[40] G. Anderegg, F. Arnaud-Neu, R. Delgado, J. Felcman, K. Popov, *Pure Appl. Chem.* **2005**, *77*, 1445–1495.
[41] a) J. Rohovec, M. Kývala, P. Vojtíšek, P. Hermann, I. Lukeš, *Eur. J. Inorg. Chem.* **2000**, 195–203; b) J. Kotek, P. Vojtíšek, I. Císařová, P. Hermann, P. Jurečka, J. Rohovec, I. Lukeš, *Collect. Czech. Chem. Commun.* **2000**, *65*, 1289–1316; c) R. Delgado, L. C. Siegfried, T. A. Kaden, *Helv. Chim. Acta* **1990**, *73*, 140–148.
[42] a) S. Chaves, R. Delgado, J. J. R. Frausto Da Silva, *Talanta* **1992**, *39*, 249–254; b) A. Bianchi, L. Calabi, C. Giorgi, P. Losi, M. Palma, P. Paoli, P. Rossi, B. Valtancoli, M. Virtuani, *J. Chem. Soc. Dalton Trans.* **2000**, 697–705.
[43] V. Kubíček, J. Kotek, P. Hermann, I. Lukeš, *Eur. J. Inorg. Chem.* **2007**, 333–344.
[44] W. P. Cacheris, S. K. Nickle, A. D. Sherry, *Inorg. Chem.* **1987**, *26*, 958–960.
[45] A. D. Sherry, J. Ren, J. Huskens, E. Brücher, É. Tóth, C. F. C. G. Geraldes, M. M. C. A. Castro, W. P. Cacheris, *Inorg. Chem.* **1996**, *35*, 4604–4612.
[46] R. Delgado, J. Costa, K. P. Guerra, L. M. P. Lima, *Pure Appl. Chem.* **2005**, *77*, 569–579.
[47] a) P. Vojtíšek, J. Rohovec, *Collect. Czech. Chem. Commun.* **2006**, *71*, 264–278; b) P. Vojtíšek, J. Rohovec, J. Klimentová, *Eur. J. Inorg. Chem.* **2008**, 3948–3956.
[48] A. Stenson, A. L. Thompson, D. Parker, *Dalton Trans.* **2006**, 3291–3293.
[49] É. Tóth, E. Brücher, I. Lázár, I. Tóth, *Inorg. Chem.* **1994**, *33*, 4070–4076.
[50] S. L. Wu, W. Horrocks, Jr., *Inorg. Chem.* **1995**, *34*, 3724–3732.
[51] P. Táborský, I. Svobodová, Z. Hnatejko, P. Lubal, S. Lis, M. Försterová, P. Hermann, I. Lukeš, J. Havel, *J. Fluoresc.* **2005**, *15*, 507–512.
[52] P. Táborský, I. Svobodová, P. Lubal, Z. Hnatejko, S. Lis, P. Hermann, *Polyhedron* **2007**, *26*, 4119–4130.
[53] Z. Piskula, I. Svobodová, P. Lubal, S. Lis, Z. Hnatejko, P. Hermann, *Inorg. Chim. Acta* **2007**, *360*, 3748–3755.
[54] a) P. Barthelemy, G. R. Choppin, *Inorg. Chem.* **1989**, *28*, 3354–3357; b) A. Beeby, I. M. Clarkson, R. S. Dickins, S. Faulkner, D. Parker, L. Royle, A. S. de Sousa, J. A. G. Williams, M. Woods, *J. Chem. Soc. Perkin Trans. 2* **1999**, 493–503.
[55] a) É. Tóth, O. M. Ni Dhubhghaill, G. Besson, L. Helm, A. E. Merbach, *Magn. Reson. Chem.* **1999**, *37*, 701–708; b) F. A. Dunand, S. Aime, S. G. Crich, G. B. Giovenzana, A. E. Merbach, *Magn. Reson. Chem.* **2002**, *40*, 87–92; c) M. Mato-Iglesias, C. Platas-Iglesias, K. Djanashvili, J. A. Peters, É. Tóth, E. Balogh, R. N. Muller, L. V. Elst, A. de Blas, T. Rodríguez-Blas, *Chem. Commun.* **2005**, 4729–4731.
[56] J. Moreau, E. Guillon, J.-C. Pierrard, J. Rimbault, M. Port, M. Aplincourt, *Chem. Eur. J.* **2004**, *10*, 5218–5232.
[57] T.-H. Yang, K. Zhou, S.-S. Bao, C.-J. Zhu, L.-M. Zheng, *Inorg. Chem. Commun.* **2008**, *11*, 1075–1078.
[58] X. Wang, T. Jin, V. Comblin, A. Lopez-Mut, E. Merciny, J. F. Desreux, *Inorg. Chem.* **1992**, *31*, 1095–1099.
[59] C. A. Chang, Y.-L. Liu, C.-Y. Chen, X.-M. Chou, *Inorg. Chem.* **2001**, *40*, 3448–3455.
[60] I. Svobodová, Z. Piskula, P. Lubal, S. Lis, P. Hermann, *J. Alloys Compd.* **2008**, *451*, 42–45.
[61] F. Benetollo, G. Bombieri, L. Calabi, S. Aime, M. Botta, *Inorg. Chem.* **2003**, *42*, 148–157.
[62] J. A. Peters, J. Huskens, D. J. Raber, *Prog. Nucl. Magn. Reson. Spectrosc.* **1996**, *28*, 283–350.
[63] C. N. Reilley, B. W. Good, R. D. Allendoerfer, *Anal. Chem.* **1976**, *48*, 1446–1458.
[64] C. Piguet, C. F. G. C. Geraldes in *Handbook on the Physics and Chemistry of Rare Earths, Vol. 33* (Eds.. K. A. Gschneider, Jr., J.-C. G. Bünzli, V. K. Pecharsky), Elsevier, Amsterdam, **2003**, Chapter 215, pp. 353–463.
[65] a) HKL Denzo and Scalepack Program Package, Z. Otwinovski, W. Minor, Nonius BV, Delft **1997**; b) Z. Otwinovski, W. Minor, *Methods Enzymol.* **1997**, *276*, 307–326.
[66] A. Altomare, G. Cascarano, C. Giacovazzo, A. Guagliardi, N. C. Burla, G. Polidori, M. Camalli, *J. Appl. Crystallogr.* **1994**, *27*, 435–435.
[67] SHELXL97. Program for Crystal Structure Refinement from Diffraction Data, G. M. Sheldrick, University of Göttingen, Göttingen **1997**.
[68] SADABS, G. M. Sheldrick, Bruker AXS Inc., Madison, WI, **2004**.
[69] SMART and SAINT, Bruker AXS Inc., Madison, WI, **2004**.
[70] A. Altomare, M. C. Burla, M. Camalli, G. Cascarano, G. Giacovazzo, A. Guagliardi, A. G. G. Moliterni, G. Polidori, R. Spagna, *J. Appl. Crystallogr.* **1999**, *32*, 115–119.
[71] PLATON—A Multipurpose Crystallographic Tool, A. L. Spek, Utrecht University, Utrecht, **2005**.

[72] a) M. Kývala and I. Lukeš, International Conference Chemometrics '95, Pardubice, Czech Republic, p. 63; full version of "OPIUM" is available on http://www.natur.cuni.cz/~kyvala/opium.html; b) M. Kývala, P. Lubal, I. Lukeš, IXth Spanish-Italian and Mediterranean Congress on Thermodynamics of Metal Complexes, Girona, **1998**.
[73] a) A. E. Martell and R. M. Smith, *Critical Stability Constants, Vols. 1–6*, Plenum Press, New York **1974–1989**; b) NIST Standard Reference Database 46 (Critically Selected Stability Constants of Metal Complexes), Version 7.0, **2003**; c) C. F. Baes, Jr., R. E. Mesmer, *The Hydrolysis of Cations.* Wiley, New York, **1976**.
[74] K. Popov, H. Ronkkomaki, L. H. J. Lajunen, *Pure Appl. Chem.* **2006**, *78*, 663–675.
[75] a) D. J. Alner, J. J. Greczek, A. G. Smeeth, *J. Chem. Soc. A* **1967**, 1205–1211; b) K. Mikkelsen, S. O. Nielsen, *J. Phys. Chem.* **1960**, *64*, 632–637; c) P. K. Glasoe, F. A. Long, *J. Phys. Chem.* **1960**, *64*, 188–190.
[76] C. Frassineti, S. Ghelli, P. Gans, A. Sabatini, M. S. Moruzzi, A. Vacca, *Anal. Biochem.* **1995**, *231*, 374–382.
[77] J. H. Forsberg, R. M. Delaney, Q. Zhao, G. Harakas, R. Chandran, *Inorg. Chem.* **1995**, *34*, 3705–3715.
[78] M. R. Willcott, R. E. Lenkinski, R. E. Davis, *J. Am. Chem. Soc.* **1972**, *94*, 1742–1744.
[79] M. Maeder, Y. M. Neuhold, G. Puxty, P. King, *Phys. Chem. Chem. Phys.* **2003**, *5*, 2836–2841.

Received: February 5, 2010
Published online: June 10, 2010

